Naval Research Laboratory

Washington, DC 20375-5320

NRL/MR/7640--02-8594

Climatology of Mountain Wave-Induced Turbulence in the Stratosphere over Central Asia: October-December 1994-2001

STEPHEN D. ECKERMANN

E.O. Hulburt Center for Space Research

May 24, 2002

REPORT DOCUMENTATION PAGE

Form Approved
OMB No. 0704-0188

1. REPORT DATE *(DD-MM-YYYY)*	2. REPORT TYPE	3. DATES COVERED *(From - To)*
May 24, 2002	Memorandum Report	September 12, 2001-October 31, 2001

4. TITLE AND SUBTITLE

Climatology of Mountain Wave-Induced Turbulence in the Stratosphere over Central Asia: October-December 1994-2001

5a. CONTRACT NUMBER

5b. GRANT NUMBER

5c. PROGRAM ELEMENT NUMBER

6. AUTHOR(S)

Stephen D. Eckermann

5d. PROJECT NUMBER

5e. TASK NUMBER

5f. WORK UNIT NUMBER

7. PERFORMING ORGANIZATION NAME(S) AND ADDRESS(ES)

Naval Research Laboratory, Code 7640
4555 Overlook Ave., SW
Washington, DC 20375-5320

8. PERFORMING ORGANIZATION REPORT NUMBER

NRL/MR/7640--02-8594

9. SPONSORING / MONITORING AGENCY NAME(S) AND ADDRESS(ES)

10. SPONSOR / MONITOR'S ACRONYM(S)

11. SPONSOR / MONITOR'S REPORT NUMBER(S)

12. DISTRIBUTION / AVAILABILITY STATEMENT

Approved for public release; distribution is unlimited.

13. SUPPLEMENTARY NOTES

14. ABSTRACT

This report summarizes experiments using the Naval Research Laboratory Mountain Wave Forecast Model (MWFM 1.1) to construct climatologies of stratospheric turbulence due to mountain wave breaking over central Asia during the months of October-December. Results are presented as standard monthly turbulence maps at three pressure (altitude) intervals in the 30-100 hPa range (heights ~16-24 km) for the years 1994-2001. Both average and maximum turbulence levels are provided.

Major findings are as follows: (1) turbulence is greatest at 70-100 hPa, and decreases significantly with height above 70-100 hPa; (2) turbulence at all heights increases on progressing into winter months (October to December); (3) geographical and year-to-year variability is large, but nonsystematic; (4) 2000 and 2001 were unusually turbulent Octobers at 70-100 hPa.

15. SUBJECT TERMS

Turbulence; Stratosphere; Central Asia; Mountain wave; Aircraft

16. SECURITY CLASSIFICATION OF:			17. LIMITATION OF ABSTRACT	18. NUMBER OF PAGES	19a. NAME OF RESPONSIBLE PERSON
a. REPORT	b. ABSTRACT	c. THIS PAGE			Stephen D. Eckermann
Unclassified	Unclassified	Unclassified	UL	52	19b. TELEPHONE NUMBER *(include area code)* 202-404-1299

Standard Form 298 (Rev. 8-98)
Prescribed by ANSI Std. Z39.18

Table of Contents

1. Introduction

This report documents results from model runs with the NRL Mountain Wave Forecast Model (MWFM) that generated monthly climatologies of turbulence due to mountain wave breaking at stratospheric pressure levels ~30-100 hPa (altitudes z~16.1-24.5 km) over central Asia. Climatologies are derived for the months of October, November and December for the years 1994-2001. Table 1 converts the atmospheric pressure intervals used throughout this report to typical flight levels and altitudes.

Pressure Level Range	Flight Levels	Approximate Altitude Range
70-100 hPa	FL 530-600	16-18.5 km
50-70 hPa	FL 600-670	18.5-21 km
30-50 hPa	FL 670-720	21-24.5 km

Table 1: Conversion of altitude ranges in hectapascals to approximate flight levels (FL530=53,000 feet) and (pressure) altitudes.

Major overall findings are summarized in the main body of the report, with details relegated to a series of Appendices. Table 2 summarizes common acronyms. Appendix A provides technical background on the MWFM, including history and heritage. We use MWFM here with daily atmospheric analysis fields from NCEP and DAO that are described in detail in Appendix A.2. The nature and interpretation of the turbulence maps generated by MWFM is described in Appendices A.3 and A.4.

A full list of results from these simulations is provided in Appendix B, with accompanying discussion and interpretation, followed by a series of 26 figures (Figures 1-26) that form the major body of model results that are interpreted and summarized below. Appendix C provides addendum results that can be added to as requests emerge for additional results for different months or years, or if different quantities or plot presentations are subsequently required.

Abbreviation	Meaning
DAO	NASA's Data Assimilation Office
GSFC	Goddard Space Flight Center
MWFM	The Mountain Wave Forecast Model
NASA	National Aeronautics and Space Administration
NCAR	National Center for Atmospheric Research
NCEP	National Centers for Environmental Prediction
NMC	National Meteorological Centers – now known as NCEP (see above)
NOGAPS	Navy Operational Global Atmospheric Prediction System
NRL	Naval Research Laboratory
NRLDC	NRL, Washington, DC
NRLMRY	NRL, Monterey, CA
NWP	numerical weather prediction

Table 2: List of some common abbreviations and acronyms used in various parts of his report.

2. Results

2.1 Monthly Turbulence Quantities

Appendix A.3.4 explains the quantities we calculate and the monthly averaging procedures: the salient features only are briefly summarized here. We run MWFM in a "hindcast" mode over central Asia at 12 Z for each day of a given month. The model issues a turbulent kinetic energy due to mountain wave breaking above various mountain ridge features, denoted $(KE)_{TURB}$ (described further in Appendix A.3.3), and these daily forecasts are stored. To summarize the turbulence characteristics in a given month, we evaluate two quantities: (1) an average level of turbulence, $(KE)_{MEAN}$, evaluated by averaging each daily $(KE)_{TURB}$ value above a given ridge over the month; (2) a maximum turbulence level for the month, $(KE)_{MAX}$, which is simply the largest daily turbulence level found above a given ridge in a given month. This gives us a measure of the typical and largest turbulence values due to mountain wave breaking in a given month.

These quantities are mapped over central Asia in Appendix B (Figures 1-26) and are discussed in detail there. Here we provide a brief summary and overview of the major findings that emerge from these maps.

Figure 2.1 summarizes, in two-dimensional histogram form, the largest values of $(KE)_{MEAN}$ and $(KE)_{MAX}$ for October, November, December as a function of atmospheric pressure level (30-50 hPa, 50-70 hPa, 70-100 hPa) and year (1994-2001). Note that there are partial results for October, 2001[1], but no

Manuscript approved January 30, 2002.

results for November or December, 2001 since these runs were performed during September and October, 2001.

2.1.1. Vertical Variations

Figure 2.1 shows a clear tendency over all months and years for the largest mean and maximum turbulence levels to occur at the lower altitude region of 70-100 hPa, with levels decreasing significantly with altitude. The values at 70-100 hPa are always larger than those higher up, indicating that the 70-100 hPa is the most turbulent altitude level from an MWFM mountain wave-breaking perspective.

2.1.2. Monthly Variations

There is a general trend in Figure 2.1 for the turbulence levels to increase at all altitudes on progressing into winter from October to December. This is particularly evident for the means (left column) at 50-70 hPa and 30-50 hPa. It is also evident at 70-100 hPa, but is masked somewhat by the large October values in 2000 and 2001[1] noted in Figure 2.1a. This reveals that 2000 and 2001 were anomalously turbulent Octobers at 70-100 hPa from a climatological perspective.

The maximum turbulence levels in a month (right column of Figure 2.1) increase even more on progressing from October to December. In December (Figure 2.1f), we see maximum values at all altitudes and most years that exceed 1-2 J m^{-3}, a nominal threshold for significant turbulence based on experience during NASA ER-2 missions (see Appendix A.3.3). Values at 70-100 hPa during December are up to an order of magnitude larger than this. Note that the values plotted in the right column of Figure 2.1 are the very largest values encountered anywhere over the central Asia region

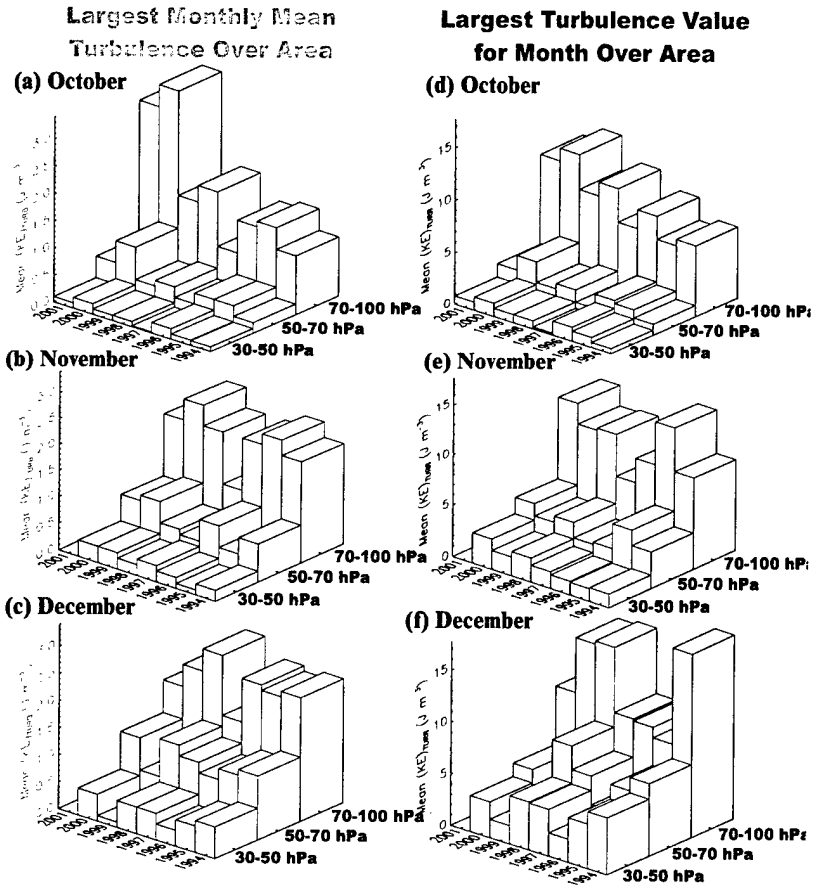

Figure 2.1: Histograms of the largest $(KE)_{MEAN}$ (left column, blue), and $(KE)_{MAX}$ (right column, red) for the months of October, November and December, plotted as a function of year (1994-2001) and pressure level (30-50 hPa, 50-70 hPa, and 70-100 hPa), based on MWFM 1.1 forecasts over central Asia in Appendix B (Figures 1-26). Note there are results for October, 2001[1], but no results for November or December, 2001.

[1] **note**: the October 2001 results were performed in late October 2001 and thus do not span the entire month since analyses for the full month were not yet online. Only the first 26 days are covered, and thus this is a partial climatology: see Appendix C.1.

during the entire month. As evident from the much lower mean values plotted in the left column, typical turbulence levels are much lighter.

2.1.3. Year-to-Year Variability

Figure 2.1 also shows that significant year-to-year variability emerges, though no systematic trend or interannual cycle is evident. For example, Figure 2.1a shows that 2000 and 2001 yielded anomalously intense mean turbulence levels at 70-100 hPa, whereas Figure 2.1f shows that largest turbulence events in December at 70-100 hPa occurred in 1994, 1998 and 1999, with 2000 showing lower levels.

Nonsystematic interannual variability is expected based on our understanding that the entire extratropical stratosphere in winter tends to vary significantly from year-to-year. Since mountain wave evolution depends on the structure of the large-scale atmosphere from the ground to the stratosphere, then year-to-year variations in mountain wave turbulence in response to year-to-year variations in the stratosphere is to be expected.

2.1.4 Geographical Variability

Geographical clustering of the turbulence over certain orographic features is discussed in depth in Appendix B. Large turbulence values do *not* always occur over certain parts of the region. An example (one of many) is Figure 14 in Appendix B, which shows mean turbulence $(KE)_{MEAN}$ for December at 50-70 hPa for 1994-1999. In 1998 and 1999 (Figure 14e, 14f), we see largest values over north-eastern Afghanistan and into Tajikistan (the Hindu Kush and Pamirs), whereas in 1994 (Figure 14a) we see the largest values occurring over central and southern Iran. Note that the scale of the color bars in these figures varies from plot to plot.

Having said that, there are regions that appear to have large turbulence values more often than others, in particular the region encompassing north-eastern Afghanistan, Tajikistan, Kyrgyzstan and the Chinese border region with the latter two countries (see, e.g., Figures 6 and 8 in Appendix B). For more details, see Appendix B.

2.1.5 Variation with Time of Day

The studies conducted here use atmospheric analyses from 12 Z only: thus, we have not investigated how the results vary during the course of a day. Since climatological diurnal variability in the atmosphere at these levels is usually small, we do not anticipate any large climatological variations in MWFM-predicted turbulence with time of day. However, since NCEP analyses are 6 hourly, MWFM could be run to investigate this effect should the need arise.

2.1.6 Reproducibility of Results

How representative are these particular findings?

First, it must be stressed that the MWFM is a simplified model (see Appendix A.1) that has received limited (though promising) ER-2 validation to date. There are undoubtedly episodes, as with all forecast models, when the model results are incorrect, and possibly badly so. For theoretical reasons, we believe that the MWFM 1.1 model tends to be systematically "overpredictive, " in the sense that it tends to overestimate turbulence levels. Improvements in the MWFM 2.1 model (see Appendices A.1.4 and A.1.5) have shown somewhat lower values compared to MWFM 1.1, though similar consistency with regard to geographical and vertical distributions of predicted turbulence. Having said that, the MWFM 1.1 and 2.1 models both have heritage and some validation in ER-2 missions, as outlined in Appendices A.1.3 and A.1.4.

The MWFM results presented here were robust to changes in the atmospheric wind and temperature sources used for the computations. In Figure 2.1 we summarized MWFM results that used NCEP reanalyses (see Appendix A.2.1) for the model runs. However, to check the sensitivity of the results to the specific wind and temperature analyses, we conducted a series of identical MWFM climatological runs that used a different set of analyses from NASA's Data Assimilation Office (DAO; see Appendix A.2.2 for details). As discussed in Appendix B.3, the MWFM-DAO results, both in terms of absolute turbulence levels and their geographical, vertical and monthly variability, were very consistent with the MWFM-NCEP results, giving us confidence that the MWFM results are not unduly sensitive to small changes in the numerical details of the atmospheric analyses and/or forecasts used.

3. Summary

The results generated here show some reproducible climatological features, such as a well-defined decrease in turbulence levels with altitude and a general increase in turbulence intensity from October through to December. Nonetheless, there is considerably year-to-year and geographical variability in the results. On the basis of these MWFM findings, it appears that daily forecasting is necessary to estimate the specifics of stratospheric turbulence due to mountain wave breaking over the central Asian region on any given day during October-December.

The major findings can be summarized as follows

- MWFM-predicted turbulence is greatest at 70-100 hPa, and decreases significantly with height (70-50 hPa), 30-50 hPa). Lightest turbulence levels occur at 30-50 hPa
- turbulence at all altitudes increases on progressing into the winter months (October to December)
- geographical and year-to-year variability in the turbulence is large, but no systematic trends or cycles emerge. There is often (though not always) large mean and maximum turbulence in the stratosphere above the mountains of the northern Hindu Kush and Pamirs (north-eastern Afghanistan, Tajikistan, Kyrgyzstan)
- The years 2000 and 2001 were unusually turbulent Octobers at 70-100 hPa over central Asia.

4. References

Bacmeister, J. T., Mountain-wave drag in the stratosphere and mesosphere inferred from observed winds and a simple mountain-wave parameterization scheme, *J. Atmos. Sci., 50*, 377-399, 1993.

Bacmeister, J. T., P. A. Newman, B. L. Gary, and K. R. Chan, An algorithm for forecasting mountain wave-related turbulence in the stratosphere, *Wea. Forecasting, 9*, 241-253, 1994.

Broutman, D., J. W. Rottman and S. D. Eckermann, A hybrid method for analyzing wave propagation from a localized source, with application to mountain waves, *Q. J. R. Meteorol. Soc., 127*, 129-146, 2001a.

Broutman, D., J. W. Rottman and S. D. Eckermann, Maslov's method for stationary hydrostatic mountain waves, *Q. J. R. Meteorol. Soc.*, (in press), 2001b.

Carslaw K. S., M. Wirth, A. Tsias, B. P. Luo, A. Dörnbrack, M. Leutbecher, H. Volkert, W. Renger, J. T. Bacmeister, E. Reimer, and T. Peter, Increased stratospheric ozone depletion due to mountain-induced atmospheric waves, *Nature, 391*, 675-678, 1998.

Carslaw, K. S., T. Peter, J. T. Bacmeister and S. D. Eckermann, Widespread solid particle formation by mountain waves in the Arctic stratosphere, *J. Geophys. Res., 104*, 1827-1836, 1999.

Dörnbrack, A., M. Leutbecher, R. Kivi, and E. Kyro, Mountain-wave-induced record low stratospheric temperatures above northern Scandinavia, *Tellus, 51A*, 951-963, 1999.

Eckermann, S. D., D. Broutman, K. A. Tan, P. Preusse and J. T. Bacmeister, Mountain waves in the stratosphere, *NRL Review 2000*, 73-86, 2000a.

Eckermann, S. D., D. Broutman, and J. T. Bacmeister, Aircraft encounters with mountain wave-induced

clear air turbulence: hindcasts and operational forecasts using an improved global model, *Preprint Volume of the Ninth AMS Conference on Aviation, Range and Aerospace Meteorology*, (in press), 2000b.

Kalnay, E., and coauthors, The NCEP/NCAR 40-year reanalysis project, *Bull. Am. Meteor. Soc.*, *77*, 437-471, 1996.

Milton, S. F., and C. A. Wilson, The impact of parameterized subgrid-scale orographic forcing on systematic errors in a global NWP model, *Mon. Wea. Rev.*, *124*, 2023-2045, 1996.

Preusse, P., A. Dörnbrack, S. D. Eckermann, M. Riese, B. Schaeler, J. T. Bacmeister, D. Broutman, and K. U. Grossmann, Space-based measurements of stratospheric mountain waves by CRISTA, 1, Sensitivity, analysis method, and a case study, *J. Geophys. Res.*, (in press), 2001.

Stefanutti, L., L. Sokolov, S. Balestri, A. R. MacKenzie, and V. Khattatov, The M-55 Geophysica as a platform for the Airborne Polar Experiment, *J. Atmos. Oceanic Technol.*, *16*, 1303–1312, 1999.

Trenberth, K. E., and D. P. Stepaniak, A pathological problem with NCEP reanalyses in the stratosphere. *J. Clim.*, in press, 2001.

Appendix A: Background Information

A.1. MWFM: Introduction, History and Heritage

A.1.1. The Problem

Surface atmospheric flow across the Earth's hills and mountains generates atmospheric gravity waves which, if the atmospheric environment is conducive, can propagate long distances (both vertically and horizontally) away from the parent orography. Much like ocean waves on a shore, these so-called *mountain waves* can *break*. When mountain waves break, they can generate severe turbulence locally that is known to be a sporadic hazard for aviation. Where and when they break depends sensitively on the wave properties and the wind and temperature environment within which the waves are propagating.

Conventional operational forecasting models provide no direct information on the appearance, extent and intensity of mountain wave-induced turbulence at flight levels. This is because the horizontal and vertical scales (wavelengths) of mountain waves, and the even smaller turbulent zones that develop within the waves, fall well below the spatial resolution limits of current numerical weather forecasting models. Even the most optimistic outlooks on advances in computing capabilities still do not offer the imminent prospect of forecast models with spatial resolutions capable of resolving mountain wave breaking processes. In the short-mid term, other somewhat different approaches to this problem are needed.

A.1.2. The MWFM Approach

The MWFM approach to this problem makes use of latest advances in theoretical understanding of mountain waves to develop detailed parameterizations of the major mountain wave dynamics deemed important for the turbulence problem. The idea is to transition this knowledge into fast numerical algorithms that can run operationally as a "postprocessor" on output from large-scale numerical weather prediction (NWP) models, thereby producing timely delivery of mountain wave turbulence forecasts a short time after conventional numerical forecast products come online. This same basic principle is used by global NWP models: as noted, these models cannot resolve breaking mountain waves, yet mountain wave breaking produces an important drag force that profoundly affects the evolution of the large-scale atmosphere. To get around this problem to some extent, global NWP models use very simple algorithms that parameterize the major drag effects of these subgrid-scale mountain wave processes [e.g., *Milton and Wilson*, 1996]. Despite their necessary simplicity (so as to not unduly slow down these computer models), these mountain wave drag parameterizations succeed in generating the necessary wave drag to improve forecast skill of global NWP models.

MWFM can be viewed as a sophisticated mountain wave parameterization algorithm, but with some important differences. Rather than running as an interactive module within the global NWP model itself, the MWFM code runs as a noninteractive remote "postprocessor" of NWP forecast products. The approach can be justified theoretically since mountain waves, once generated, essentially decouple from the large-scale atmosphere, so that the background atmosphere affects the waves' propagation but the waves do not greatly affect the evolving background atmosphere until the waves dissipate and produce drag. Thus, to first order, we can use NWP model output to model realistic wave propagation through the forecast atmosphere, without needing to worry about large feedback effects of the waves on the background atmosphere that modify the wave propagation environment.

This greatly simplifies the approach and offers a number of practical advantages. It allows MWFM algorithms to be as sophisticated as deemed necessary, dictated only by computational speed concerns associated with the model itself running on it's own remote computer system. In contrast, the complexity of mountain wave drag parameterizations is usually limited by stringent constraints on

computing turnaround time of the full NWP model forecasts. The MWFM approach also allows the model to focus in detail on those processes important to the specific turbulence generation problem for which it is designed, as opposed to mountain wave drag parameterizations, which focus solely on the drag force that the NWP model requires, and de-emphasizes or ignore all other "extraneous" processes that add to the computing burden.

A.1.3. MWFM 1.0

The Mountain Wave Forecast Model was initiated in the early 1990s as a simple research model to study the role of mountain waves in the momentum budget of upper regions of the atmosphere [*Bacmeister*, 1993]. The results it generated showed considerable promise, perhaps for transition as a sophisticated new mountain wave drag parameterization. Shortly thereafter, however, the code was modified and transitioned into an operational turbulence forecasting configuration, in response to a need from NASA for turbulence forecast products to aid safe planning of stratospheric science flights with the ER-2 aircraft, a modified U2 spy plane. The stratosphere, due to its extreme dryness and stability, lacks many of the sources of turbulence familiar to aviators in the lower atmosphere (e.g., storms, convection, unstable jet streams). Indeed, severe turbulence events encountered by ER-2/U2 pilots at cruise altitudes (heights ~15-20 km) often occurred over mountains. Surface flow distortions or lee cyclogenesis by topography do not extend to mid-stratospheric altitudes and so cannot explain these turbulent events. Mountain waves, however, can propagate to these altitudes and break, but as mentioned above, no means for forecasting them existed. The description of the model formulation and it's modification for forecasting stratospheric mountain wave turbulence for the ER-2, along with some results and post analysis of forecast performance during ER-2 science flights, are provided by *Bacmeister et al.* [1994].

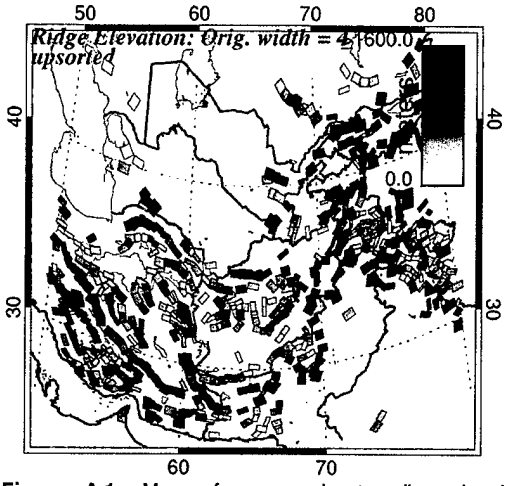

Figure A.1: Map of mesoscale two-dimensional ridgelets for topography of the central Asian region. Color bar scale (top right) depicts surface elevations of these ridge features in the range 0-1600 meters. Surface flow over these ridges is used to generate mountain waves in the MWFM.

As discussed by *Bacmeister et al.* [1994], the model performed well in forecasting mountain wave-induced turbulence for ER-2 flights in the middle stratosphere (cruise levels ~15-20 km, pressure levels ~50-100 hPa). The model has since been incorporated routinely as a flight planning tool for NASA science missions that involve ER-2 flights near significant mountainous terrain. Thus, since the early 1990s, this turbulence forecasting version of the model has been maintained and enhanced at NRLDC in a series of periodic upgrades. However, the core algorithms (discussed below) remained largely unchanged until recently. In preparation for some more substantial planned changes to the MWFM (see section 1.1.4), during 1998 it was decided to name this entire project "The Mountain Wave Forecast Model" (MWFM), and to designate this initial basic operational model as MWFM Version 1.0 (MWFM 1.0). MWFM Version 1 algorithms continue to be maintained and are used in a variety of forecasting and analysis applications. For details on recent applications, see *Eckermann et al.* [2000a, 2000b].

One key feature of the MWFM Version 1 model is that it uses a series of quasi-two-dimensional "ridgelets" derived from a detailed mathematical decomposition of the Earth's topography. Each ridgelet possesses a characteristic height, width, orientation and quality of fit that provide a useful set of parameters for defining the characteristics of a mountain wave generated by surface flow across such a feature. Mesoscale width ridges from the database for the central Asia region are plotted in Figure A.1.

Another key feature is the use of hydrostatic mountain wave equations to model and track the vertical propagation of each mountain wave from its parent ridge through the forecast atmospheric winds and temperatures. State-of-the-art criteria are used to locate when and where in the atmosphere these waves break, and how severely, thereby providing the turbulence forecast (more details are provided in section A.3.3). This process is repeated iteratively to formulate maps of mountain wave-induced turbulence intensities at various altitudes from all the relevant mountainous terrain in a preselected region. These regions can be arbitrarily small or large, potentially out to fully hemispheric or even global scales. Such capabilities can be achieved because the model algorithms are fairly simple and streamlined numerically and thus can be run very fast, an essential feature of any operational forecasting code.

A.1.4. MWFM 2.0

Despite some success [*Bacmeister et al.*, 1994], it was also recognized from the outset that MWFM 1.0 is a highly simplified model that neglects (on the basis of initial simplicity and computational speed) a host of contributing atmospheric effects that can be very important for accurately describing mountain waves and the turbulence they produce in certain circumstances. However, adding these effects without drastically complicating (and slowing down) the code required thought and research, which was conducted in-house at NRLDC. At the same time interest in the MWFM from a variety of external agencies continued to increase significantly. Some of this interest centered on forecasting applications that were never anticipated when the model was first created: e.g., forecasting mountain wave temperature decreases that produce polar stratospheric clouds and potentially large associated ozone loss in Arctic winter [*Carslaw et al.*, 1998, 1999]. To forecasts all these effects better, and given some key in-house research breakthroughs, we decided in 1998 to begin a new phase in MWFM development, leading to a new code known as MWFM Version 2.

Given the success of the basic MWFM "postprocessor" approach, it was decided to retain this approach for MWFM Version 2. However, we decided to significantly overhaul the algorithms describing mountain wave generation, propagation and breakdown into turbulence. The major change was to replace the two-dimensional hydrostatic irrotational mountain wave equations with a much more general set of three-dimensional mountain wave ray-tracing equations, which include the effects of planetary rotation, nonhydrostatic dynamics, dynamical and convective wave breaking criteria, and so on [*Marks and Eckermann*, 1995]. These improved equations have some important beneficial effects, including an ability to describe three-dimensional mountain "ship wave" patterns, vertical reflection/trapping of mountain wave energy, downstream (lee) propagation due to nonhydrostatic or inertial-scale effects, and many others effects besides. *Broutman et al.* [2001a, 2001b] describe some theoretical studies that demonstrate the ability of the ray-based formulation to reproduce quite complex three-dimensional mountain wave effects, while *Eckermann et al.* [2000a, 2000b] describe initial beneficial impacts of inclusion of first simplified versions of these ray-based algorithms into an operational MWFM 2.0 code. Most importantly, the ray tracing method is attractive for the MWFM project because a great deal of sophisticated wave physics can be incorporated via computationally efficient (i.e. fast) numerical ray-tracing algorithms. Thus, additional wave physics can be added without seriously compromising the turnaround time of the MWFM operational forecast cycle.

A first operational version of the new ray-based code (MWFM 2.0) was initiated in late 1999 in preparation for a major NASA science campaign with the ER-2. To be based in Kiruna, Sweden, the SAGE III Ozone Loss and Validation Experiment (SOLVE) presented a series of logistical and scientific challenges that required the most extensive MWFM forecasts to date. Firstly, Kiruna is based in the heart of the northern Norwegian Mountains, which are known to be a strong source of mountain waves for the stratosphere during winter [e.g., *Dörnbrack et al.*, 1999]. Furthermore, these mountain waves produced intense turbulent buffeting during stratospheric flights over the region with the Russian M-55 Geophysica during January 1997 [*Stefanutti et al.*, 1999]. Thus serious pre-mission questions existed as to whether Kiruna presented a safe stratospheric flying environment for the ER-2, given its

structural vulnerability to turbulence and the additional difficulties of flights in 24-hour darkness (polar night) within the remote Arctic environment. MWFM 1.0 monthly mean mountain wave turbulence climatologies were calculated over Kiruna [*Eckermann et al.*, 2000b] and were found to be generally light, but with considerable day-to-day, month-to-month and interannual variability. In this report, the same sort of climatological turbulence calculations that we supplied for SOLVE ER-2 deployments are repeated and extended here over central Asia (Appendix B). The pre-mission SOLVE turbulence climatologies for Kiruna reinforced the importance of daily operational forecasts for safe flight planning.

Consequently, a detailed operational forecasting campaign was conducted for NASA during SOLVE, with daily mountain wave forecasts running at NRLDC and delivered via the web for flight planners in Kiruna during the entire winter of 1999-2000 (November-April)[2]. These forecasts included not just mountain wave-induced turbulence forecasts at typical cruise altitudes for NASA's ER-2 (50-70 hPa) and DC-8 (200-250hPa), but also included first detailed forecasts of mountain wave temperature drops that could form polar stratospheric clouds. The latter was a major science goal of the SOLVE mission and thus another key determinant for flight planning. This presented a challenge for MWFM, since ER-2 flights to intercept mountain wave-induced PSCs were desirable, but only if the waves producing these clouds were nonturbulent: turbulent mountain waves always needed to be avoided. Both MWFM 1.0 and MWFM 2.0 forecasts were provided, the latter for the first time during a NASA mission, the former to provide a standard product with heritage during NASA missions that could be used to compare with the new 2.0 output.

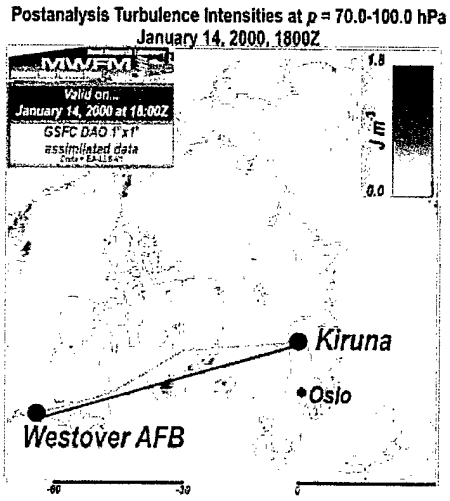

Figure A.2: Example of planned "straight shot" ER-2 ferry flight from Westover AFB to Kiruna on January 14, 2000 (navy curve) and the rerouted flight path (aqua curve) based on MWFM 2.0 turbulence forecasts for that day. MWFM 2.0 post-analysis turbulence is also plotted based on NASA DAO atmospheric wind and temperature analyses for that day, showing that forecast turbulence persisted in the MWFM analysis run, and was avoided on the rerouted flight.

Preliminary results of this work were reported by *Eckermann et al.* [2000a, 2000b]: full scientific writeup of the findings is being prepared for publication. An example of the type of MWFM 2.0 turbulence forecast that led to a reroute of the ER-2 ferry flight from Westover AFB to Kiruna is shown in Figure A.2. In all, ~16 ER-2 flights were undertaken during SOLVE, most long duration (~4-8 hours, including ferry flights), and some of these flights were rerouted as in Figure A.2 to avoid forecast turbulence. Despite flights over major mountainous terrain (Norwegian Mountains, Greenland, Iceland, Urals, Novaya Zemlya, Spitzbergen), no severe turbulence events were encountered during any of the flights.

A.1.5. MWFM 1.1 & MWFM 2.1

Both the MWFM 1.0 and 2.0 models have recently been transitioned to 1.1 and 2.1 versions, respectively. These changes reflect major changes to the MWFM software, but do not reflect any significant changes in the fundamental dynamics and physics underpinning each model. A brief description of the changes is provided for completeness.

Both the 1.0 and 2.0 models are coded in IDL (MWFM 2.0 also uses FORTRAN routines). When MWFM 1.0 was developed, it made extensive use of a repository of IDL library routines maintained at NASA GSFC. These routines controlled many of the scientific operations, as well as the plotting and mapping of results. While MWFM 2.0 was developed as an offshoot of MWFM 1.0 and

[2] http://uap-www.nrl.navy.mil/dynamics/html/mwfm_solve1.html

was designed to run within it (thus using some of these library routines), a conscious effort was made during MWFM 2.0 development to make this code more "standalone." In particular, wherever possible MWFM 2.0 made use of intrinsic IDL analysis and mapping routines rather than those of the external GSFC IDL libraries. In addition to the standalone functionality, this change also enabled us to make use of the regular upgrades in functionality to these intrinsic IDL routines that appear with each new software release.

This proved to be useful: however, it had the undesirable side effect of making the MWFM 1.0 and 2.0 codes progressively more dissimilar from one another, due to the former using static GSFC library routines, the latter acquiring increased functionality with each release of improved intrinsic IDL routines. In mid-2001, it was decided to transition both the MWFM 1.0 and 2.0 to use intrinsic IDL software modules wherever possible. The most notable effect of this transition, completed in October 2001, was a major change in the appearance of forecast maps issued by the MWFM 1.0 code, changes we view as almost uniformly positive. Thus the end result of these changes is mainly cosmetic and the forecast numbers from both the MWFM 1.0 & 2.0 codes are essentially the same as those from the MWFM 1.1 and 2.1 codes, respectively.

A.1.6. The Future: MWFM Version 3

Basic research and development of new codes with potential for transition to the MWFM continues at NRLDC. In particular, in October 2001 we commenced a new formal research initiative explicitly dedicated to this goal: up until then, all of this development work had been conducted sporadically on a task-to-task basis. Thus we anticipate ongoing developments and improvements to MWFM that will eventually lead to a Version 3 code. Briefly, some of the issues to be addressed include:

- Improved specifications of the Earth's topography for the model, using latest digital elevation maps
- Inclusion of effects such as wind speed curvature and moisture to improve forecasts at tropospheric flight levels
- Treatment a low-level nonlinear breaking effects
- Use full capability of the ray method, treating caustics and near field effects based on recent theoretical developments using the Maslov method [*Broutman et al.*, 2001b]
- Efforts to test and validate the code operationally using flight data, to focus on where/when the code works well and when it doesn't, to better target the R&D effort

A.2. Atmospheric Analysis Fields

A.2.1. NCEP 40-Year Reanalysis Fields

In this multi-year climatological work, we have chosen to use global wind and temperature analyses from the National Centers for Atmospheric Research (NCEP)/NCAR 40-year reanalysis project [*Kalnay et al.*, 1996]. The main reason for choosing these particular analysis fields is that they provide an uninterrupted unchanging analysis throughout the period 1994-2001, giving us greater confidence that any interannual changes we see in the MWFM output are due to real effects rather numerical changes due to a change in the atmospheric analysis procedures from one year to another. Another reason for this choice is that these are recent reanalysis fields that use a "state of the art" modern data assimilation system. These NCEP reanalysis fields come gridded globally at 2.5°x2.5° resolution at 17 pressure levels from the ground up to 10 hPa (z~35 km), and are issued 4 times per day (0,6,12,18Z). In all work in this report we work only with the analyses at 12Z.

A.2.2. DAO Analysis Fields

While the NCEP reanalysis fields provide a continuous set of wind and temperature assimilations of a specific kind throughout 1994-2001 that are "state of the art" and reliable, no analysis is perfect, since they all use global models to assimilate scattered and varied observations. For NCEP reanalyses, some questions exist as to the some potentially spurious divergence signals in the uppermost stratospheric levels, most notably over topography [*Trenberth and Stepaniak*, 2001]. Detailed work at NRLDC with the MWFM over the Andes Mountains in a project to model stratospheric mountain waves seen in satellite data also revealed a tendency for the NCEP reanalysis zonal winds at the uppermost stratospheric levels (10 hPa and below) to be systematically weaker than those seen in other analyses [*Preusse et al.*, 2001]. Given our focus on mountainous terrain and the known sensitivity of mountain wave forecasts to details in the synoptic scale winds, it was decided to conduct "check" simulations with other analyses to check the fidelity and robustness of the MWFM results. This is somewhat akin to a crude "ensemble" forecasting process, such that an MWFM 1.1 forecast of a given kind is repeated using a background atmosphere with somewhat different initial conditions.

We choose analyses from NASA's Data Assimilation Office (DAO) for this purpose, since these analyses should rectify some of the potential problems with NCEP reanalyses noted above. The DAO focuses on stratospheric assimilations, with output extending to much higher altitudes (~0.4 hPa, z~55 km) than NCEP reanalyses. Since numerical analysis errors tend to congregate near the upper model boundary, such high-altitude analyses largely eliminate the potential for numerical errors at the mid stratospheric levels 30-100 hPa considered here. Furthermore, a great deal of research effort is devoted to improved stratospheric assimilation, so that these winds and temperatures are "state of the art" for the stratosphere.

However, these DAO analyses have their own shortcomings that the NCEP analyses do not have. First, there is no standard set of DAO analyses that span 1994-2000: a number of different types of DAO analyses exist throughout these years. This is because the DAO is a research analysis center rather than a purely operational center, and thus it changes it's analysis procedures as research breakthroughs occur and does not currently go back to "reanalyze" the previous analyses with the improved system as NCEP do. Furthermore, the quality of the tropospheric analyses in DAO may not be as good as NCEP reanalyses, given the stratospheric focus of the DAO (NCEP has more tropospheric levels). Both tropospheric and stratospheric winds and temperatures are important for the MWFM stratospheric forecasting. In the simulations conducted here we use the "STRATF" analyses, which span the 1994-1997 period but were phased out after 1998 for more modern analysis procedures. The DAO STRATF analyses are issued on a 2.5°x2° global grid at 18 standard pressure levels from the ground (1000 hPa) to 0.4 hPa (z~55 km).

As for the NCEP fields, we use only the 12Z DAO analysis fields in the MWFM modeling for this report.

A.3. Interpreting the MWFM 1.1 Turbulence Forecasts

A.3.1. MWFM 1.1 Forecast Specifics

The MWFM 1.1 forecasts detailed in this report are conducted within the central Asian longitude interval 50°-80° E and latitude interval 25°-45°N. Mountain waves are initialized in the standard hydrostatic MWFM 1.1 procedure described by *Bacmeister et al.* [1994]. A narrow version of the ridge database (Figure A.1) is used to focus on the subgridscale meso-scale mountain waves that are believed to be most relevant to mountain wave-induced turbulence.

A.3.2. Plot/Map Format

Mountain waves in the MWFM 1.1 code are two-dimensionalized with respect to the major axis of the parent ridge, and yield plane hydrostatic wave solutions that propagate purely vertically above the mountain (see *Bacmeister et al.* [1994] for details). This has the useful property of allowing us to characterize the wave and its amplitude according to the location of it's parent ridge feature, since in this version of the model the stratospheric mountain wave lies directly above it. While a simplification, in practice the mountain wave is generally located fairly close to its parent ridge geographically: horizontal dispersion away from the ridge is modeled more accurately by the MWFM 2.1 model. The MWFM 2.1 model is not used here since it is in development and is harder to run in a multiyear climatological configuration currently. Thus the precise ridge-fixed locations of turbulence in the figures in Appendix B should not be taken too literally. Nonetheless, the basic geographical distributions and clustering of turbulence activity should be considered significant.

Thus the plots presented and discussed in Appendix B use a map and plot format that looks very similar to the map of the mesoscale ridge database shown in Figure A.1. The difference is that the color scales, rather than showing the elevation of the ridge feature as in Figure A.1, show the intensity of turbulence produced by mountain wave breaking at stratospheric altitudes above the mountain. This plot/map format makes it easier to associate regions of strong turbulence with given geographical regions and mountain ranges.

A.3.3 Quantification and Significance of Turbulence Intensities

MWFM predictions of mountain wave-induced turbulence are plotted as maps of "turbulent kinetic energy," although the magnitude of the numbers cannot be interpreted directly using turbulence theory. The calculation follows the method outlined in *Bacmeister et al.* [1994]. Briefly, each mountain wave has associated with it a vertical flux of horizontal momentum density, ϕ, that remains constant with height until the waves break, based on a standard convective saturation criterion. When waves break, momentum flux is dissipated to return the wave to marginal stability, and it is assumed that the dissipated momentum flux density is transferred into turbulent kinetic energy. Within the MWFM, this is achieved as follows. First, we consider two successive pressure (vertical) levels from the large-scale analysis winds and temperatures (e.g., NCEP), denoted p_i and p_{i+1}, where i is an integer vertical level index from the NCEP or DAO analysis pressure grids. A typical example here is a calculation of turbulence in the 50-70 hPa range (e.g., Figure 10), where $p_i = 70$ hPa and $p_{i+1} = 50$ hPa. The turbulent kinetic energy at 50-70 hPa is calculated according to the proportionality formula

$$(KE_{TURB})_{p_i}^{p_{i+1}} \propto \phi(p_{i+1}) - \phi(p_i). \qquad \text{(A1)}$$

In MWFM, we use a proportionality constant of 1, for simplicity only: the real proportionality would be more complex than this.

One reason we have retained the simplified calculation (A1) is that such calculations go back many years and span a number of NASA science missions with the stratospheric ER-2 aircraft. Turning any theoretical turbulence index into an accurate aircraft-buffeting index is extremely difficult, since the way turbulence affects any given aircraft is highly airframe specific and probably only fully assessable using detailed aerodynamic drag calculations for a given airframe and atmospheric pressure. The calculation (A1), though simple, has been compared during forecasts and postanalyses to a number of ER-2 turbulence episodes that have been associated with mountain waves [*Bacmeister et al.*, 1994; *Eckermann et al.*, 2000a, 2000b]. While limited, this has enabled us to develop some working MWFM thresholds for "significant" turbulence for the ER-2 based on comparisons between ER-2 turbulence episodes and MWFM forecast/hindcast output using equation (A1). This heritage leads us to persist with the calculation method (A1) in both MWFM 1.1 and 2.1 for now, and for the future until more detailed validation data can be found that to allow us to construct and test more complex turbulence metrics.

Based on this heritage, a crude working threshold for "significant" turbulence for the ER-2 has been developed: forecast values > 1 J m^{-3} are considered significant Several significant turbulence episodes for the ER-2 yielded MWFM 1.0 and 1.1 predictions in the 2-6 J m^{-3} range. The 1 J m^{-3} criterion was also the working threshold used during forecasting for the SOLVE campaign in Kiruna during the winter of 1999-2000 (see section A.1.4).

A.3.4. Climatological Averaging Procedures and Monthly Turbulence Measures

Two specific monthly turbulence indices based on analysis of daily MWFM 1.1 $(KE)_{TURB}$ calculations (see section A.3.3) are presented in the climatological monthly turbulence maps presented in Figures 1-26 in Appendix B.

A.3.4.1. Monthly Mean Turbulence Intensities

This is a simple unweighted linear average of each daily $(KE)_{TURB}$ calculation using equation (A1), performed for mountain wave breaking above each ridge feature in Figure A.1. This calculation gives the monthly mean turbulence intensity above each ridge feature due to mountain wave breaking.

A.3.4.2. Maximum Turbulence Intensity During the Month

While mean turbulence levels in a given month are useful basic climatological indicators, they are not the most useful things to study from a flight planning and safety perspective. Of more relevance is the magnitude of the very largest turbulence events that occur in a given month, which are the events of most concern for aircraft in the region. Thus, we calculate the maximum value of mountain wave-induced turbulent kinetic energy $(KE)_{TURB}$ for each day of the month. These turbulence values of course tend to be much larger than the monthly means.

A.3.4.3. Probability/Frequency of Given Turbulence Levels

Given a reliable working threshold for "significant" turbulence, we can also calculate the number of days in any given month where the MWFM-calculated turbulence over the mountain exceeds this threshold level. We can then calculate monthly probabilities or frequencies of occurrence of these threshold-exceeding events. Such data give an indication of how probable hazardous turbulence events might be. While we have calculated such probabilities for a range of thresholds for 1994-2000 at various altitudes over central Asia, we have chosen not to list all these results in Appendix B in the interest of keeping the report to a manageable length: nonetheless, they can be supplied upon request.

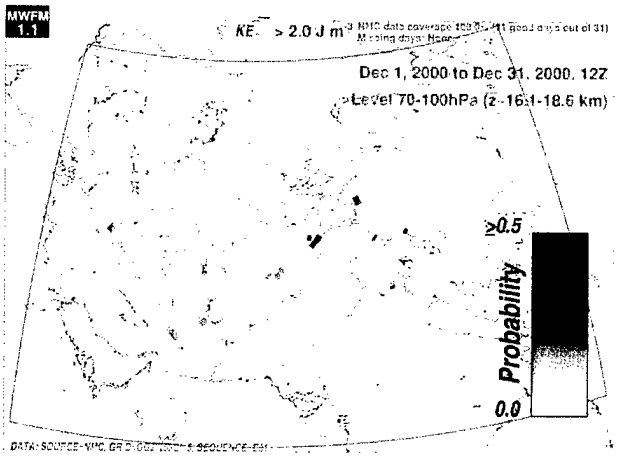

Figure A.3: Plot of probability of mountain wave-induced turbulence occurrences >2 J m^{-3} at 70-100 hPa during December 2000, based on MWFM 1.1 daily hindcasts at 12Z using NCEP reanalysis winds and temperatures. A value of 0.5 indicates a 50% probability on any given day

For completeness, we show one example of such a monthly mean turbulence occurrence map in Figure A.3. This map shows the occurrence rate of turbulent kinetic energy values > 2 J m^{-3}, a threshold considered significant for ER-2 flights based on limited previous experience (see section A.3.3). We see significant occurrence probabilities at 70-100 hPa for December 2000 over north-eastern Afghanistan, the China-Tajikistan border, as well as smatterings of significant occurrence probabilities elsewhere.

Appendix B: Monthly Turbulence Maps

B.1. MWFM 1.1-NCEP Climatologies for 2000

We begin by forming monthly climatologies of mountain wave-induced turbulence as computed using the MWFM 1.1 model coupled to NCEP reanalysis winds and temperatures at 12Z for October, November and December, 2000. The work in section B.1 serves as initial case studies to introduce the results and the way in which turbulence output from the model is averaged, plotted and distributed geographically. Fuller results for the years 1994-1999 follow in section B.2.

All Figures 1-26 are collated in order at the end of Appendix B, and are introduced and discussed sequentially in the following sections. We plot here the mean turbulence kinetic energies (see section A.3.4.1) and maximum turbulent kinetic energies (section A.3.4.2) due to mountain wave breaking. For further background on model, calculations, and plot format, see Appendix A.

B.1.1. October 2000

Figure 1 shows the October, 2000 monthly mean turbulence intensities due to hindcast mountain wave breaking at three selected atmospheric altitude intervals: 70-100 hPa (heights z~16.1-18.6 km; top row), 50-70 hPa (z~18.6-21 km; middle row), and 30-50 hPa (z~21-24.5 km; bottom row). These choices are based on a stratospheric aircraft that typically cruises in the 50-70 hPa interval, but may episodically drift to slightly higher or lower pressure levels. Monthly mean turbulent energy KE_{TURB} due to mountain wave breaking is plotted in the left column, while the peak daily turbulence levels encountered during the month at each ridge location is plotted in the right column (see section A.3.4 for background). All values are scaled according to the color bar on the bottom-right of each plot: *it is important to note* when studying these figures that the scale ranges on these color bars vary from plot to plot.

On inspecting Figure 1, we see that the largest monthly mean turbulence intensities (left column) are found at 70-100 hPa, and decrease in intensity significantly with altitude, with mean values at 30-50 hPa more than an order of magnitude smaller than those at 70-100 hPa. The largest daily turbulence intensities during October, plotted in the right column of Figure 1, are (naturally enough) considerably larger than the monthly mean values in the left column, typically by a factor of ~3-5. This indicates considerable day-to-day variability in turbulence intensity. Again, these peak turbulence intensities are greatest at 70-100 hPa and smallest at 30-50 hPa.

The largest turbulence values tend to cluster in a region of north-eastern Afghanistan, northern Pakistan, Tajikistan and Kyrgyzstan. There is also a smattering of significant activity over the border region of Iran and Turkmenistan.

B.1.2. November 2000

Figure 2 shows same plot sequence for computations during November, 2000. Monthly means at 70-100 hPa (Figure 2a) fall in the 0-2 J m^{-3} range, values somewhat smaller than for October (Figure 1a). Like October, however, November turbulence shows a similar decrease in intensity with altitude at 50-70 hPa and 30-50 hPa. Interestingly, the maximum turbulence value at 70-100 hPa for November (Figure 2b) is somewhat larger than for October (Figure 1a), suggesting that turbulence production was more intermittent in November, since the peak value is larger but the monthly mean is smaller. Maximum turbulence intensities at upper levels (50-70 hPa, Figure 2d; 30-50 hPa, Figure 2f) are larger than during October. Again, a decrease with altitude is evident.

As for October, activity in November is concentrated over north-eastern Afghanistan and Tajikistan, although during November we see somewhat larger values over central Afghanistan as well.

B.1.3. December 2000

Figure 3 shows the same plot sequence for computations during December, 2000. Mean turbulence at 70-100 hPa (Figure 3a) is slightly lighter again than in November (Figure 2a) and around half the intensity from October (Figure 1a). At upper levels (Figure 3c, 3e), however, the mean values are larger than those in November and October. Similar trends occur for the maximum daily turbulence values during the month (right column): the December peak at 70-100 hPa (Figure 3b) is smaller than for October and November, but larger than the October-November values at upper levels (50-70 hPa and 30-50 hPa). We note that the largest mean and maximum turbulence values at 70-100 hPa occur over north-eastern Afghanistan. The same general decrease in mean and maximum turbulence intensities with increasing height (decreasing pressure) that was seen in October and November also persists in December. Rather than most activity occurring in and around the Hindu Kush and Pamirs, during December we see increased activity over Iran.

B.2. MWFM 1.1-NCEP Climatologies for 1994-1999

The analyses for October-December 2000 and part of October 2001 provide initial indications of the monthly mountain wave-induced turbulence characteristics predicted by the MWFM 1.1 model over central Asia in the middle stratosphere at pressure levels in the 30-100 hPa range (heights ~16-24 km). Some reproducible trends emerged, such as a general decrease in turbulence intensities with increasing altitude (decreasing pressure). What is unclear is how reproducible other features, such as absolute turbulence intensities and geographical and monthly variability, are from year to year. Thus, in this section we collate and discuss MWFM 1.1-NCEP climatologies derived for 6 successive earlier years spanning 1994-99. With 7 years of data (1994-2000), the aim is to identify any reproducible seasonal and geographical trends over the months October-December.

B.2.1. 70-100 hPa: October 1994-1999

B.2.1.1. Mean Turbulence

Figure 4 shows mean turbulence intensities at 70-100 hPa during October for the years 1994 to 1999 (Figures 4a-4f). The largest mean turbulence intensities (see color bars) range from a minimum of 0.8 J m^{-3} (October 1997) to a maximum of 1.8 J m^{-3} (October 1998). All these values are considerably smaller than the 3.4 J m^{-3} found in October 2000 (Figure 1a) and the 3.0 J m^{-3} for October 1-26, 2001 (Figure C.1a). This suggests that 2000 and 2001 had unusually turbulent Octobers at 70-100 hPa over central Asia.

In addition to variability in these mean values, the geographical distribution of mean turbulence activity in Figure 4 varies from year to year. Large values occur over north-eastern Afghanistan (Hindu Kush and Pamirs) in October 1995 and 1998, whereas in October 1997 turbulence values in these regions are extremely low, with more activity in southern Afghanistan, Pakistan and Iran.

B.2.1.2. Maximum Turbulence

Similar trends emerge in the maximum daily turbulence intensities for October at 70-100 hPa, plotted in Figure 5. The largest of these values lie in the range 6.9-9.9 J m^{-3}, values smaller than the ~12 J m^{-3} found for October, 2000 (Figure 1b) and 10.7 J m^{-3} for October 1-26, 2001 (Figure C.1b). This reinforces the impression from section B.2.1.1 above that 2000 and 2001 had unusually turbulent stratospheres at 70-100 hPa in October over central Asia. Areas of intensity in Figure 5 vary from year to year: largest values are seen over north-eastern Afghanistan in October 1996, whereas in October 1997 largest values occur in the south and west, similar to features in the monthly means (Figure 4)

B.2.2. 70-100 hPa: November 1994-1999

B.2.2.1. Mean Turbulence

Figure 6 maps mean turbulence intensities at 70-100 hPa during November for the years 1994 to 1999 (Figures 6a-6f). The largest means (see color bars) range from a minimum of 1.0 J m^{-3} (November 1997) to a maximum of 2.4 J m^{-3} (November 1999). These values fall within the range of the 2.0 J m^{-3} in November 2000 (Figure 2a). These means are generally larger than the October means in Figure 4.

Geographical distributions of these means in Figure 6 vary quite a bit from year to year. In November, 1994, largest mean values are observed over south-western Iran, whereas in November 1996 and 1998 there is almost no detectable turbulence over Iran. In November 1998 largest mean values are confined to a narrow zone near the Tajikistan-China border. During November 1997 the largest values occur near China, Pakistan and Tajikistan (Figure 6d), whereas in October 1997 (Figure 4d) turbulence values in these regions are extremely low, with more activity in southern Afghanistan, Pakistan and Iran. This suggests significant month-to-month variations in the geographical clustering.

B.2.2.2. Maximum Turbulence

Largest November turbulence occurrences at 70-100 hPa in Figure 7 lie in the range 6.6-13.3 J m^{-3}, values within the range of the ~12.7 J m^{-3} found in November, 2000 (Figure 2b). Geographical clustering of the regions of peak values vary from year-to-year, and resemble those seen in the means in Figure 6.

B.2.3. 70-100 hPa: December 1994-1999

B.2.3.1. Mean Turbulence

Largest values of monthly mean turbulence levels at 70-100 hPa during December for the years 1994 to 1999 (Figures 8a-8f) range from 1.5 J m^{-3} (December 1997) to 2.6 J m^{-3} (December 1998). These values fall within the range of the 1.8 J m^{-3} value found earlier in December 2000 (Figure 3a). These means are generally larger than the means in October (Figure 4) and November (Figure 6), indicating an increase in turbulence intensities with progression into the winter months.

Geographical variability in these means from year to year is significant in Figure 8, although it is not as extensive as for November (Figure 6). Mean values over north-eastern Afghanistan are fairly significant in all years 1994-1999.

B.2.3.2. Maximum Turbulence

Values of maximum turbulence intensity in December at 70-100 hPa (Figure 9) attain largest values (see color bars) in the range 9.5-17.7 J m^{-3}. The ~10.4 J m^{-3} found in December, 2000 (Figure 3b) falls within the low side of this range. These peak values are noticeably larger than values found for October (Figure 5) and November (Figure 7). Geographical clustering of the maximum values varies from year to year: in December 1994 (Figure 9a) the large value of 17.7 J m^{-3} occurred over Iran, whereas in December 1998-1999 large turbulence excursions were preferentially clustered over the Tajikistan-China region and Tajikistan-Afghanistan border regions, with much smaller values over Iran in these years.

B.2.4. 50-70 hPa: October 1994-1999

B.2.4.1. Mean Turbulence

Figure 10 maps monthly mean turbulence intensities at the 50-70 hPa flight levels (heights z~18.6-21 km) during October for the years 1994-1999. The largest of these mean values fall in the 0.2-0.4 J m^{-3} range, values considerably smaller than the 0.9 J m^{-3} found for October 2000 (Figure 1c), suggesting that October 2000 was anomalously turbulent at 50-70 hPa as well (see section B.2.1). Initial

assessments of October, 2001 (Figure C.1c) yield means of ~0.5 J m^{-3}, indicating that 2001 was also a fairly turbulent October, though not as turbulent as October 2000.

Year-to-year variations in the geographical clustering of the large mean turbulence values are evident in Figure 10. October 1995 (Figure 10b) shows largest means over the greater Tajikistan region, whereas in October 1997 (Figure 10d) there is little if any turbulence over Tajikistan, and the largest mean values are located further south over southern Pakistan and Iran.

B.2.4.2. Maximum Turbulence

Maximum daily turbulence intensities at 50-70 hPa in October (Figure 11) attain largest values (see color bars) in the range 0.8-2.2 J m^{-3}, values smaller than the ~3.5 J m^{-3} found for October, 2000 (Figure 1d). This again indicates that 2000 was an anomalously turbulent October at these altitudes. Year-to-year geographical variations are somewhat similar to those seen for the means in Figure 10: for example, turbulence over Iran shows similar year-to-year variability.

B.2.5. 50-70 hPa: November 1994-1999

B.2.5.1. Mean Turbulence

Mean turbulence intensities at 50-70 hPa during November for the years 1994 to 1999 are plotted in Figure 12. Largest values range from ~0.4 J m^{-3} in November 1995 to ~0.9 J m^{-3} in November 1999. The 0.8 J m^{-3} found in November 2000 (Figure 2c) also falls within this range. These November means are generally larger than those in October (Figure 10).

There are considerable year-to-year variations in the geographical clustering of these means. For example, in November, 1994, largest mean values are observed over Iran, whereas very little activity is found over Iran in November 1996, a similar finding to the November 70-100 hPa results in section B.2.2.1 (Figure 6). Here mean values over north-eastern Afghanistan and Tajikistan are always on the high side of values for the central Asia region.

B.2.5.2. Maximum Turbulence

Peak daily turbulence intensities at 50-70 hPa during November (Figure 13) attain largest values (see color bars) in the range 2.4-5.0 J m^{-3}. The value of 4.5 J m^{-3} found in November, 2000 (Figure 2d) falls within this range. These values are considerably larger than the October 2000 values at 50-70 hPa, plotted previously in Figure 11. This indicates that November is a more turbulent month than October. Geographical clustering is similar to that seen in the means in Figure 12.

B.2.6. 50-70 hPa: December 1994-1999

B.2.6.1. Mean Turbulence

Figure 14 plots December monthly means for 1994-1999: largest values range from 0.6 J m^{-3} (December 1999) to 1.3 J m^{-3} (December 1998). These values fall within the range of the 1.2 J m^{-3} value found at 50-70 hPa in December 2000 (Figure 3c). These means are larger than those at similar levels in October (Figure 10) and November (Figure 12), indicating a general increase in turbulence intensities produced by mountain wave breaking into the winter months.

Geographical clustering of these means varies from year to year: large values over Iran in December 1994 (Figure 14a) are almost totally absent in December 1996: similar features were noted at these altitudes in November (Figures 12a, 12c). Large mean turbulence levels are seen in December in most years over north-eastern Afghanistan.

B.2.6.2. Maximum Turbulence

Maximum daily turbulence intensities for December 1994-1999 are plotted in Figure 15. The largest turbulent excursions range from 2.9-8.3 J m^{-3} (see color bars), a wide range of values comparable

with the 4.8 J m^{-3} peak in December, 2000 (Figure 3d). The magnitude of these peak excursions during December is noticeably larger than those found at these pressure levels during October (Figure 11) and November (Figure 13), indicating that December is the most intensely turbulent month of the three at 50-70 hPa. Geographical clustering of the regions of peak values varies from year to year.

B.2.7. 30-50 hPa: October 1994-1999

B.2.7.1. Mean Turbulence

Figure 16 plots mean turbulence intensities for October at the 30-50 hPa flight level interval for the years 1994 to 1999. Largest values from the color bars fall in the range 0.02-0.2 J m^{-3}, values much smaller than the means found at lower levels during October (see Figures 4 and 10). The mean value of 0.02 J m^{-3} found in Figure 16d indicates that the 30-50 hPa levels during October 1997 received no significant turbulence from mountain wave breaking (see also section B.2.7.2 below). Given the generally low values, geographical variations from year to year are probably not very significant.

B.2.7.2. Maximum Turbulence

Figure 17 maps the peak daily values of mountain wave-induced turbulence intensities at 30-50 hPa during October for the years 1994-1999. These peak occurrences from year to year fall in the range 0.2-1.4 J m^{-3}, within the range of the 1.3 J m^{-3} found for October, 2000 (Figure 1f) and 0.8 J m^{-3} found for October 1-26, 2001 (Figure C.1f). Again, these maximum monthly intensities are much smaller than those found during October at 70-100 hPa (Figure 5) and 50-70 hPa (Figure 11). The maximum 30-50 hPa turbulence intensities over central Asia during October 1997 was 0.2 J m^{-3}, indicating (as the means in Figure 16 showed) that the stratosphere at 30-50 hPa over central Asia during October 1997 was almost totally unaffected by mountain wave-induced turbulence. Given the generally low values, geographical variations from year to year are probably not very significant, although the largest values seem to occur over Tajikistan and Kyrgyzstan.

B.2.8. 30-50 hPa: November 1994-1999

B.2.8.1. Mean Turbulence

Figure 18 maps mean turbulence intensities at 30-50 hPa for November for the years 1994 to 1999. Maximum values (see color bars) fall in the range 0.09-0.3 J m^{-3}. These values are much lower than November values found at lower levels (see Figures 6 and 12). The mean values here are slightly larger than 30-50 hPa values during October (Figure 16), although the values are still quite light. The largest means seem to occur preferentially over Tajikistan.

B.2.8.2. Maximum Turbulence

Figure 19 maps the maximum daily values of mountain wave-induced turbulence at 30-50 hPa during November from 1994-1999. The largest values (see color bars) lie in the range 1.2-2.3 J m^{-3}, values significantly larger than those typically found at these levels in the previous month of October (see Figure 17). Nonetheless, these values are much smaller than November turbulence levels at lower flight altitudes (Figures 7 and 13). The largest values in Figure 19 seem to occur over north-eastern Afghanistan, Tajikistan, Kyrgyzstan and the Chinese border with these countries.

B.2.9. 30-50 hPa: December 1994-1999

B.2.9.1. Mean Turbulence

Figure 20 plots monthly mean mountain wave-induced turbulence intensities at 30-50 hPa in December for the years 1994-1999. Largest mean values (see color bars) lie in the range 0.1-0.6 J m^{-3}, values that are larger than those found at 30-50 hPa during November (Figure 18) and October (Figure

16). This again indicates that December is more turbulent at 30-50 hPa than October and November. As noted in previous months, the mean values at 30-50 hPa are considerably smaller than those found lower down at 50-70 hPa (Figure 14) and 70-100 hPa (Figure 8). Largest means seem to occur to the north (Tajikistan, Kyrgyzstan), although reasonably large mean values over Iran arose in December 1994 (Figure 20a).

B.2.9.2. Maximum Turbulence

Maximum daily turbulence intensities during December for years 1994-1999 are plotted in Figure 21. The largest of these turbulent excursions (see color bars) fall in the range 1.8-5.6 J m^{-3}, values considerably larger than those encountered at 30-50 hPa during November (Figure 15) and October (Figure 9), further reinforcing the impression of December as the most turbulent month at 30-50 hPa. Nonetheless, these peak turbulence intensities are still smaller in intensity than those that occur during December at lower altitudes (see Figures 17 and 19).

Significant differences in the geographical distributions of these peak turbulence events occur from year to year. For example, largest values occur over southern Iran and northern Pakistan and India during December 1994 (Figure 21a). In December 1998 large values are seen again over northern Pakistan-India as well as north-eastern Afghanistan, Tajikistan and Kyrgyzstan, whereas little turbulence is found over Iran.

B.3. MWFM 1.1-DAO Climatologies for 1994-1999

No set of analysis winds and temperatures provides a perfect representation of the atmosphere in any given region: all have strengths and weaknesses. NCEP reanalyses are considered a good source of atmospheric winds and temperatures for this work, given their continuity through 1994-2001 and the use of a modern state-of-the-art analysis system. However, as discussed in section A.2.2, potential weak nesses of the NCEP reanalyses for this work include some concerns about stratospheric fields in the uppermost stratospheric levels at and below 10 hPa, particularly over steep mountains.

For these reasons, we repeat some selected climatological calculations here using analysis winds and temperatures from NASA's Data Assimilation Office (DAO), specifically their "STRATF" analysis. As discussed in section A.2.2, these analyses should have a generally better stratosphere than the NCEP analyses, though perhaps a somewhat less accurate troposphere. These analyses span 1994-1997 only and so we show results for these years only rather than the 1994-1999 period covered for the NCEP simulations.

We consider only a small subset of simulations to see whether the NCEP-based and DAO-based MWFM 1.1 climatologies are comparable or not. Here we focus solely on monthly mean turbulence intensities.

B.3.1. 70-100 hPa: October 1994-1997

Figure 22 plots monthly mean turbulence intensities for October 1994-1997 based on MWFM 1.1 model runs using the daily DAO STRATF analyses at 12Z. The corresponding simulations using NCEP 12Z reanalysis were given in section B.2.1.1 (Figure 4), and we compare the results in these two figures. There is excellent consistency between the two climatologies. Largest values in Figure 22 are 1.0 J m^{-3} (1994), 2.0 J m^{-3} (1995), 1.5 J m^{-3} (1996), and 0.6 J m^{-3} (1997), which compare well in magnitude with the corresponding NCEP-based values from Figure 4 of 1.1 J m^{-3} (1994), 1.5 J m^{-3} (1995), 1.4 J m^{-3} (1996), and 0.8 J m^{-3} (1997). Furthermore, the geographical distributions in each year are very similar in the NCEP and DAO climatologies: for example, in both Figures 4 and 22, activity is scattered around southern Pakistan and northern India in 1994 (panel a), whereas extensive activity over Iran is evident in 1997 (panel d). In short, the DAO climatologies reproduce all the major features and general turbulence intensities seen in the NCEP climatologies.

B.3.2. 70-100 hPa: November 1994-1997

Figure 23 plots monthly mean turbulence intensities for November 1994-1997 based on MWFM 1.1 model runs using the DAO STRATF analyses. The corresponding simulations using NCEP reanalysis were given earlier in section B.2.2.1 (Figure 6). There is general consistency between the two climatologies. Largest values in Figure 23 are 2.9 J m^{-3} (1994), 1.8 J m^{-3} (1995), 2.9 J m^{-3} (1996), and 1.5 J m^{-3} (1997), which compare reasonably with the corresponding NCEP-based values from Figure 6 of 1.9 J m^{-3} (1994), 2.2 J m^{-3} (1995), 2.0 J m^{-3} (1996), and 1.0 J m^{-3} (1997). The geographical distributions in each year are very similar in the NCEP and DAO climatologies: for example, in both Figures 6 and 23 there is considerable activity over Iran in 1994, but more activity over Afghanistan, northern Pakistan, northern India, and Tajikistan in 1995 and 1997. Again, the DAO climatologies in Figure 23 reproduce the same general features in the turbulence intensity maps that were seen in the corresponding NCEP climatologies in Figure 6.

B.3.3. 70-100 hPa: December 1994-1997

Figure 24 plots the monthly mean turbulence intensities for December 1994-1997 based on MWFM 1.1 model runs using the DAO STRATF analyses. The corresponding simulations using NCEP reanalysis were given earlier in section B.2.3.1 (Figure 8). There is general consistency between the two climatologies. Largest values in Figure 24 are 3.8 J m^{-3} (1994), 2.2 J m^{-3} (1995), 2.9 J m^{-3} (1996), and 1.6 J m^{-3} (1997), which compare reasonably with the corresponding NCEP-based values from Figure 8 of 2.3 J m^{-3} (1994), 2.2 J m^{-3} (1995), 2.3 J m^{-3} (1996), and 1.5 J m^{-3} (1997). The geographical distributions in each year are very similar in the NCEP and DAO climatologies: for example, in both Figures 8 and 24 large mean turbulence values are concentrated over northern India, whereas in 1994 there is also significant mean turbulence over Iran. In short, the DAO and NCEP maps are quite similar.

B.3.4. 50-70 hPa: December 1994-1997

We now stay with December simulations and look at results for this month at higher altitudes. Figure 25 plots the mean turbulence intensities for December 1994-1997 at 50-70 hPa, based on MWFM 1.1 model runs using the DAO STRATF analyses at 12Z. The corresponding simulations using NCEP reanalysis were given earlier in section B.2.6.1 (Figure 14). There is again quite reasonable consistency between the two climatologies. Largest values in Figure 25 are 1.8 J m^{-3} (1994), 1.8 J m^{-3} (1995), 1.0 J m^{-3} (1996), and 1.1 J m^{-3} (1997), which compare reasonably with the corresponding NCEP-based values from Figure 14 of 1.2 J m^{-3} (1994), 1.2 J m^{-3} (1995), 0.9 J m^{-3} (1996), and 1.1 J m^{-3} (1997). Furthermore the geographical distributions in each year are very similar in the NCEP and DAO climatologies: for example, 1994 reveals large values over Iran and northern India, while 1996 shows weakening of the activity over Iran.

B.3.5. 30-50 hPa: December 1994-1997

Figure 26 plots the mean turbulence intensities for December 1994-1997 at 30-50 hPa, based on MWFM 1.1 model runs using the DAO STRATF analyses at 12Z. The corresponding simulations using NCEP reanalysis were given earlier in section B.2.9.1 (Figure 20). There is again quite reasonable consistency between the two climatologies. Largest values in Figure 26 all fall within a rather constant range of 0.5-0.6 J m^{-3}, which compare very well with the corresponding NCEP-based values from Figure 20 of 0.6 J m^{-3} (1994), 0.5 J m^{-3} (1995), 0.3 J m^{-3} (1996), and 0.5 J m^{-3} (1997). Furthermore the geographical distributions in each year are quite similar: for example, 1997 reveals large values north-eastern Tajikistan.

Appendix C: Addendum – Additional/Future MWFM Results

This appendix lists addendum results generated after the initial set of climatological MWFM 1.1 results shown in Appendix B. This appendix will also serve to show results from later updated versions of the report, where additional results that might be requested will be listed.

C.1. October 1-26, 2001: NCEP Reanalyses

At the time of writing (October 29, 2001), NCEP reanalysis winds and temperatures had been issued for 1-26 October, 2001. Here we use these recently issued analyses to conduct a partial monthly MWFM turbulence climatology for October, 2001 using the same plot sequence as in sections B.1.1-B.1.3. Since MWFM 1.1 and 2.1 forecasts have been issued daily for this region throughout October, 2001 using both NCEP and NOGAPS forecast fields, postanalysis of this time period is particularly interesting and gives some basis for baselining climatologies in other months and years. This is our first addendum figure (Figure C.1), all of which will be listed in Appendix C as new data and analysis come online and new results for other months are generated upon request.

Figure C.1 plots the same plot sequence as Figures 1-3 for the period 1-26 October, 2001. Somewhat similar to October 2000 (Figure 1a), mean turbulence levels at 70-100 hPa during 1-26 October, 2001 (Figure C.1a) are ~3 J m^{-3} and concentrated above the mountains of the Hindu Kush and Pamirs: intensities elsewhere are considerably lighter. At upper levels (50-70 hPa and 30-50 hPa) values are considerably lighter than during October-December, 2000. Again, a clear decrease in turbulence intensities with increasing height is evident. Maximum turbulence intensities in the month (right column of Figure C.1) are all smaller than those found during October-December, 2000.

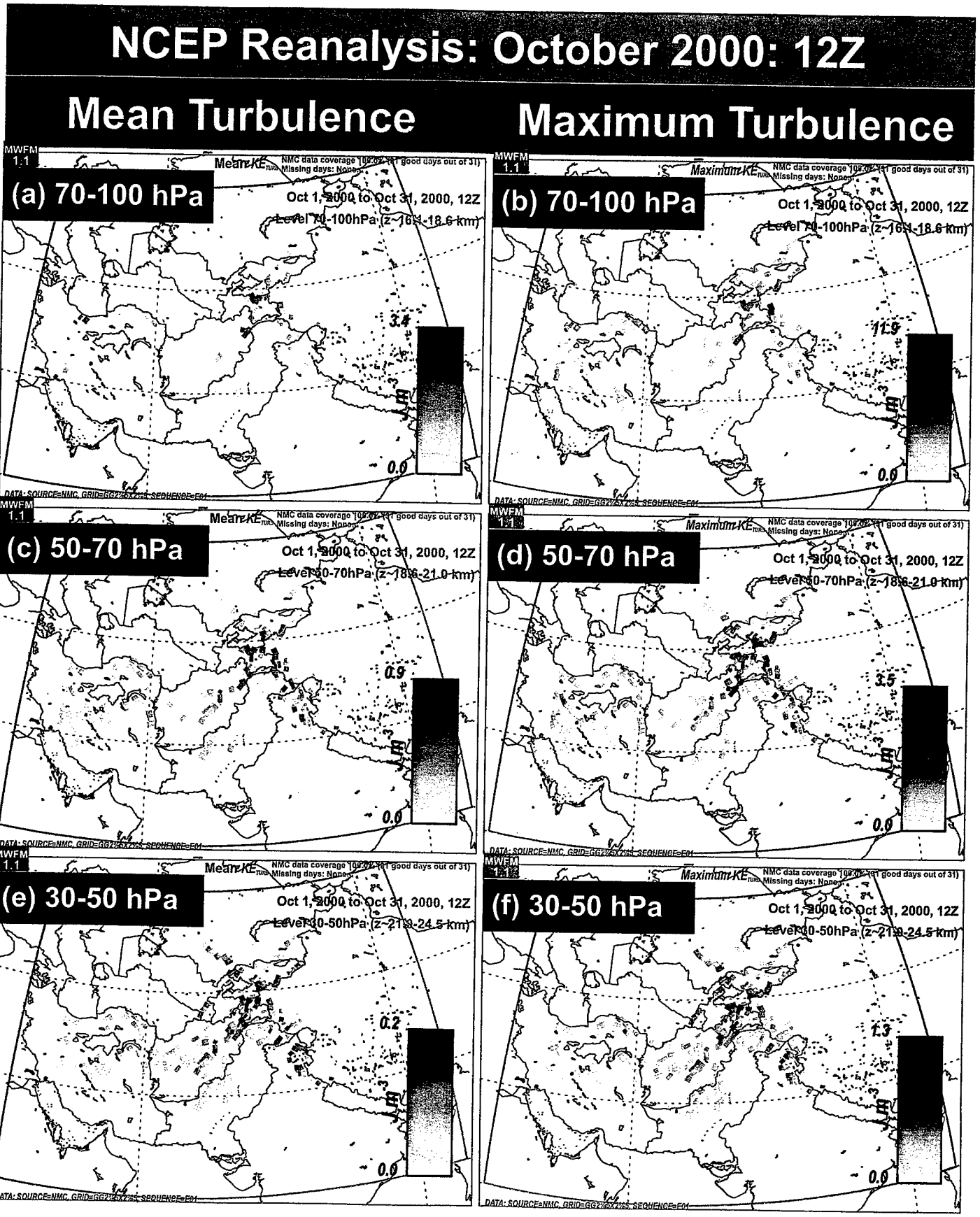
NCEP Reanalysis: October 2000: 12Z
Mean Turbulence
Maximum Turbulence
(a) 70-100 hPa
(b) 70-100 hPa
(c) 50-70 hPa
(d) 50-70 hPa
(e) 30-50 hPa
(f) 30-50 hPa
Oct 1, 2000 to Oct 31, 2000, 12Z
Level 70-100hPa (z~16.1-18.6 km)
Level 50-70hPa (z~18.6-21.0 km)
Level 30-50hPa (z~21.0-24.5 km)
3.4
11.9
0.9
3.5
0.2
1.3
0.0
MWFM 1.1

Figure 1

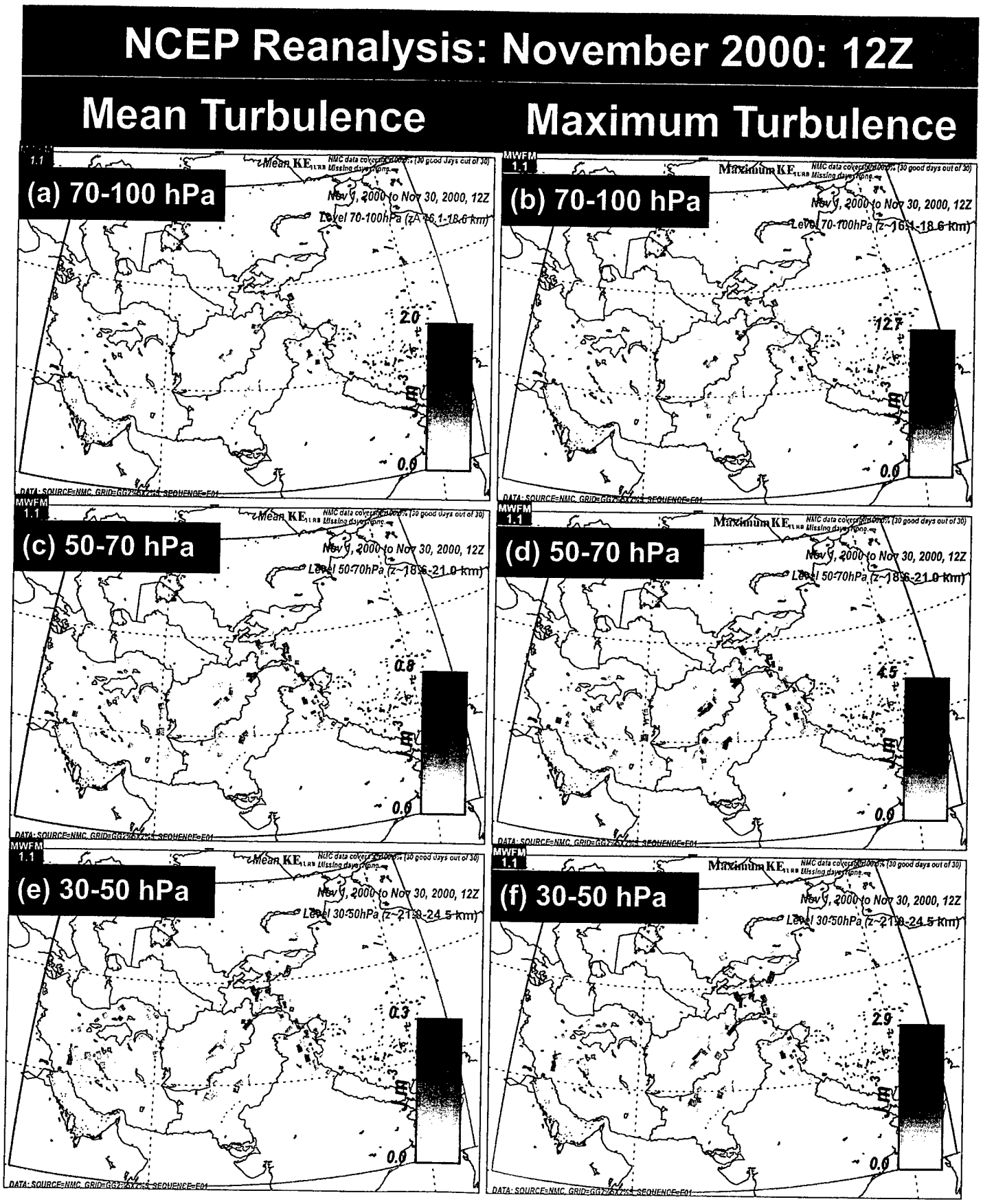
NCEP Reanalysis: November 2000: 12Z
Mean Turbulence
Maximum Turbulence
(a) 70-100 hPa
(b) 70-100 hPa
(c) 50-70 hPa
(d) 50-70 hPa
(e) 30-50 hPa
(f) 30-50 hPa
Nov 1, 2000 to Nov 30, 2000, 12Z
2.0
0.0
12.7
0.8
4.5
0.3
2.9

Figure 2

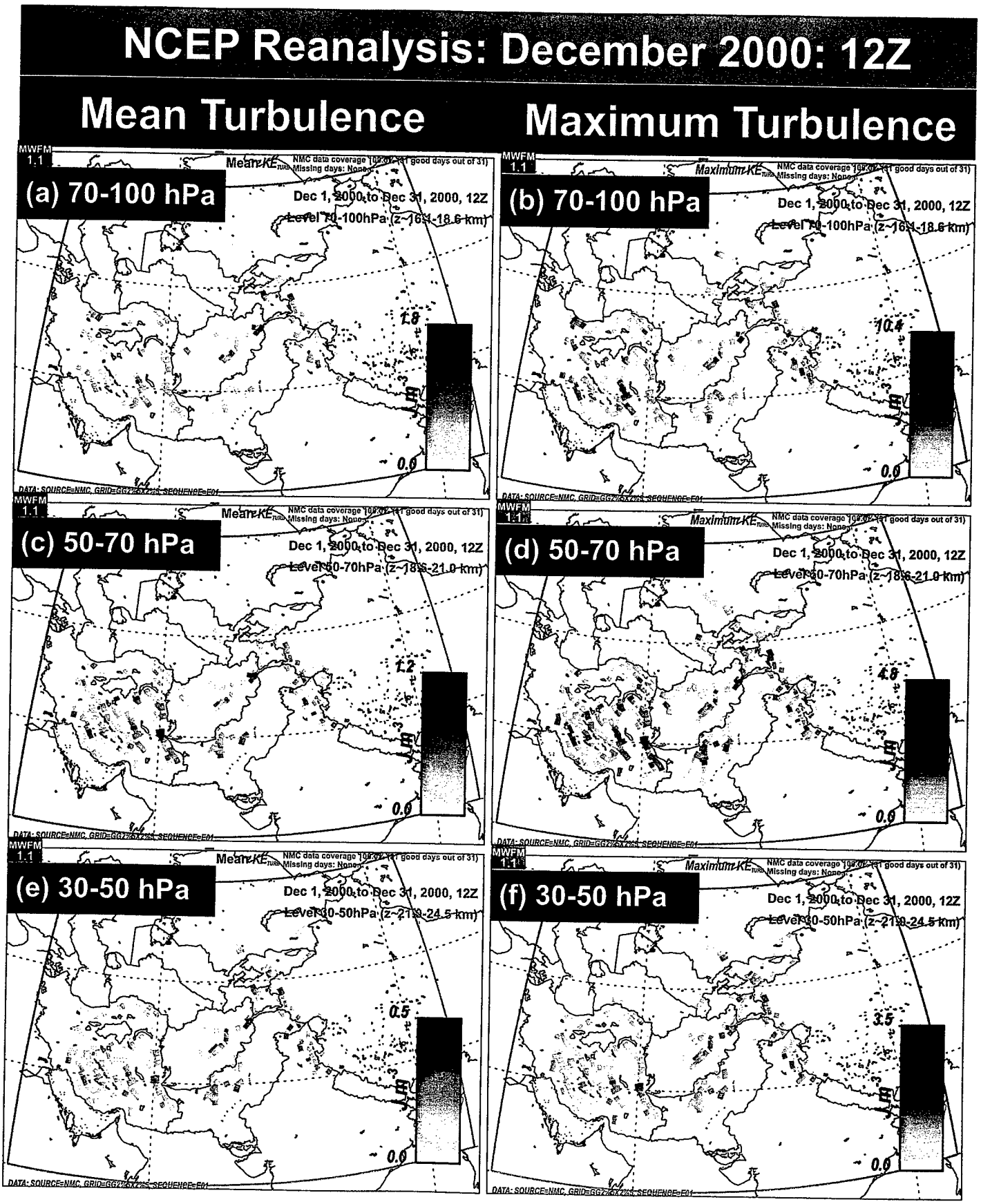
NCEP Reanalysis: December 2000: 12Z
Mean Turbulence
Maximum Turbulence
(a) 70-100 hPa
(b) 70-100 hPa
(c) 50-70 hPa
(d) 50-70 hPa
(e) 30-50 hPa
(f) 30-50 hPa
Dec 1, 2000 to Dec 31, 2000, 12Z
Level 70-100hPa (z~16.4-18.6 km)
Level 50-70hPa (z~18.6-21.0 km)
Level 30-50hPa (z~21.0-24.5 km)
MWFM 1.1
Mean KE TURB
Maximum KE TURB
NMC data coverage 100.0% (31 good days out of 31)
Missing days: None
1.8
0.0
10.4
1.2
4.8
0.5
3.5

Figure 3

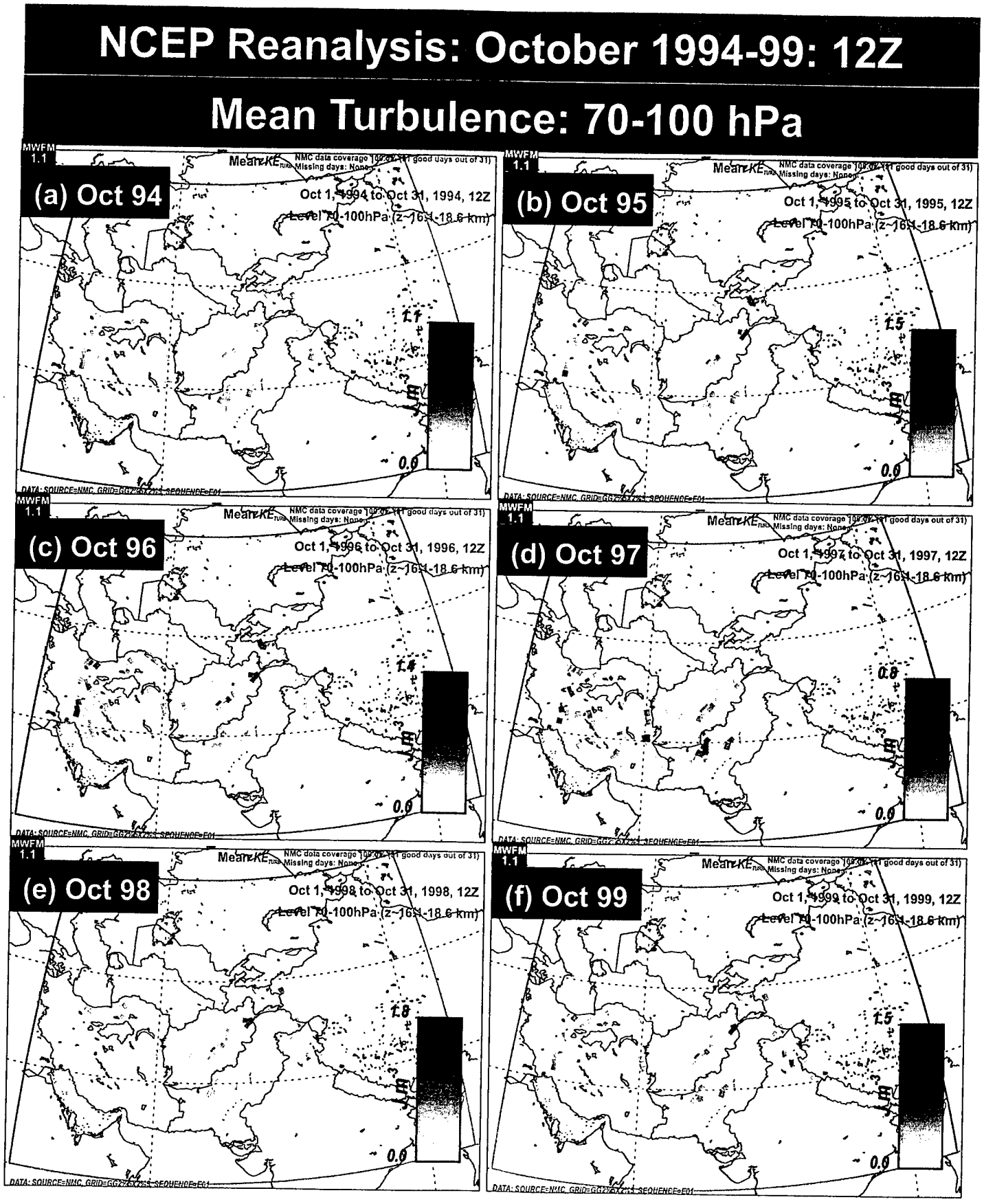
NCEP Reanalysis: October 1994-99: 12Z
Mean Turbulence: 70-100 hPa
(a) Oct 94
Oct 1, 1994 to Oct 31, 1994, 12Z
(b) Oct 95
Oct 1, 1995 to Oct 31, 1995, 12Z
(c) Oct 96
Oct 1, 1996 to Oct 31, 1996, 12Z
(d) Oct 97
Oct 1, 1997 to Oct 31, 1997, 12Z
(e) Oct 98
Oct 1, 1998 to Oct 31, 1998, 12Z
(f) Oct 99
Oct 1, 1999 to Oct 31, 1999, 12Z
Level 70-100hPa (z~16.1-18.6 km)
MWFM 1.1

Figure 4

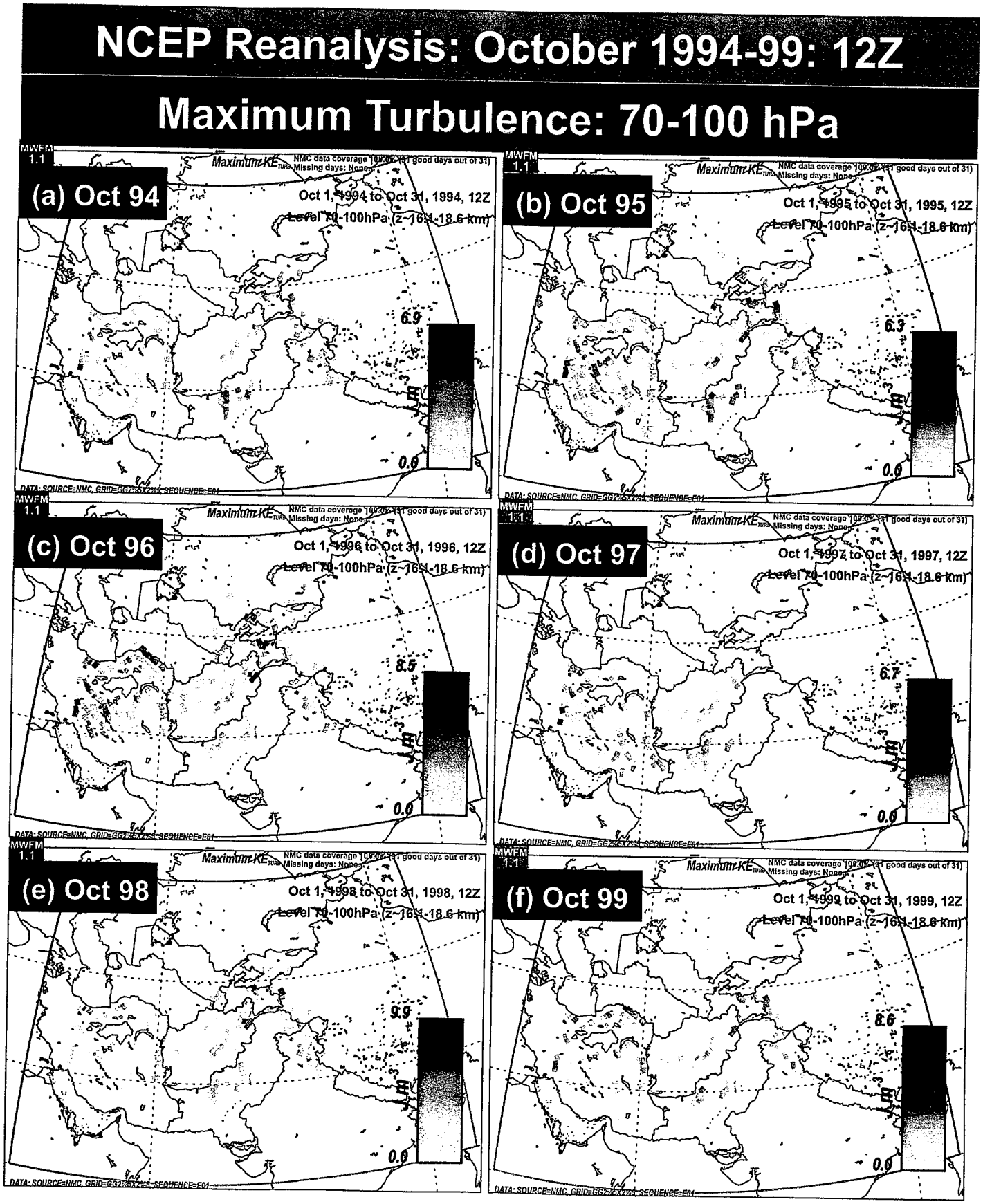
NCEP Reanalysis: October 1994-99: 12Z
Maximum Turbulence: 70-100 hPa
(a) Oct 94
Oct 1, 1994 to Oct 31, 1994, 12Z
Level 70-100hPa (z~16.1-18.6 km)
6.9
0.0
(b) Oct 95
Oct 1, 1995 to Oct 31, 1995, 12Z
Level 70-100hPa (z~16.1-18.6 km)
6.3
0.0
(c) Oct 96
Oct 1, 1996 to Oct 31, 1996, 12Z
Level 70-100hPa (z~16.1-18.6 km)
8.5
0.0
(d) Oct 97
Oct 1, 1997 to Oct 31, 1997, 12Z
Level 70-100hPa (z~16.1-18.6 km)
6.7
0.0
(e) Oct 98
Oct 1, 1998 to Oct 31, 1998, 12Z
Level 70-100hPa (z~16.1-18.6 km)
9.9
0.0
(f) Oct 99
Oct 1, 1999 to Oct 31, 1999, 12Z
Level 70-100hPa (z~16.1-18.6 km)
8.6
0.0

Figure 5

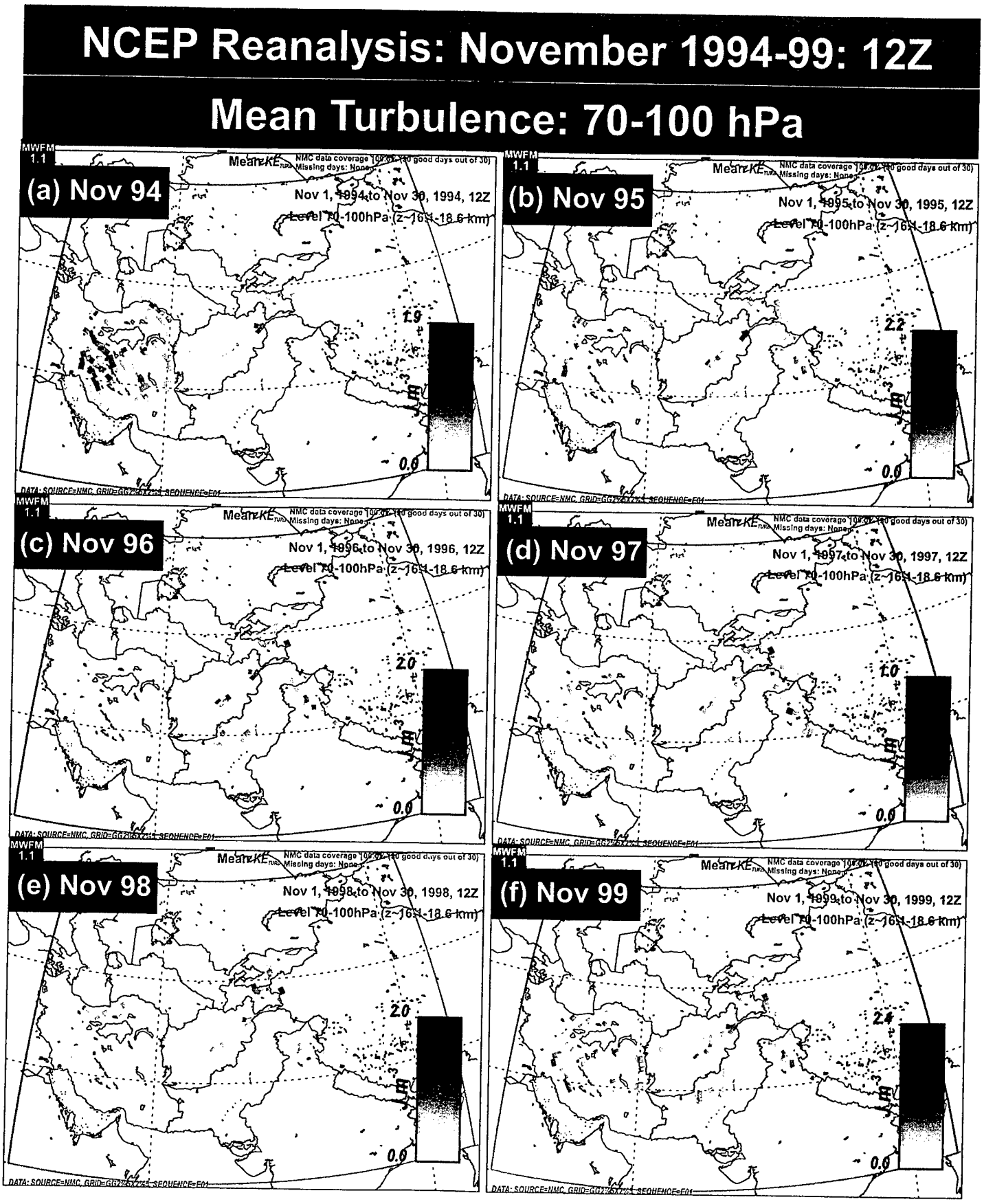
NCEP Reanalysis: November 1994-99: 12Z
Mean Turbulence: 70-100 hPa
(a) Nov 94
Nov 1, 1994 to Nov 30, 1994, 12Z
Level 70-100hPa (z~16.1-18.6 km)
(b) Nov 95
Nov 1, 1995 to Nov 30, 1995, 12Z
Level 70-100hPa (z~16.1-18.6 km)
(c) Nov 96
Nov 1, 1996 to Nov 30, 1996, 12Z
Level 70-100hPa (z~16.1-18.6 km)
(d) Nov 97
Nov 1, 1997 to Nov 30, 1997, 12Z
Level 70-100hPa (z~16.1-18.6 km)
(e) Nov 98
Nov 1, 1998 to Nov 30, 1998, 12Z
Level 70-100hPa (z~16.1-18.6 km)
(f) Nov 99
Nov 1, 1999 to Nov 30, 1999, 12Z
Level 70-100hPa (z~16.1-18.6 km)

Figure 6

NCEP Reanalysis: November 1994-99: 12Z

Maximum Turbulence: 70-100 hPa

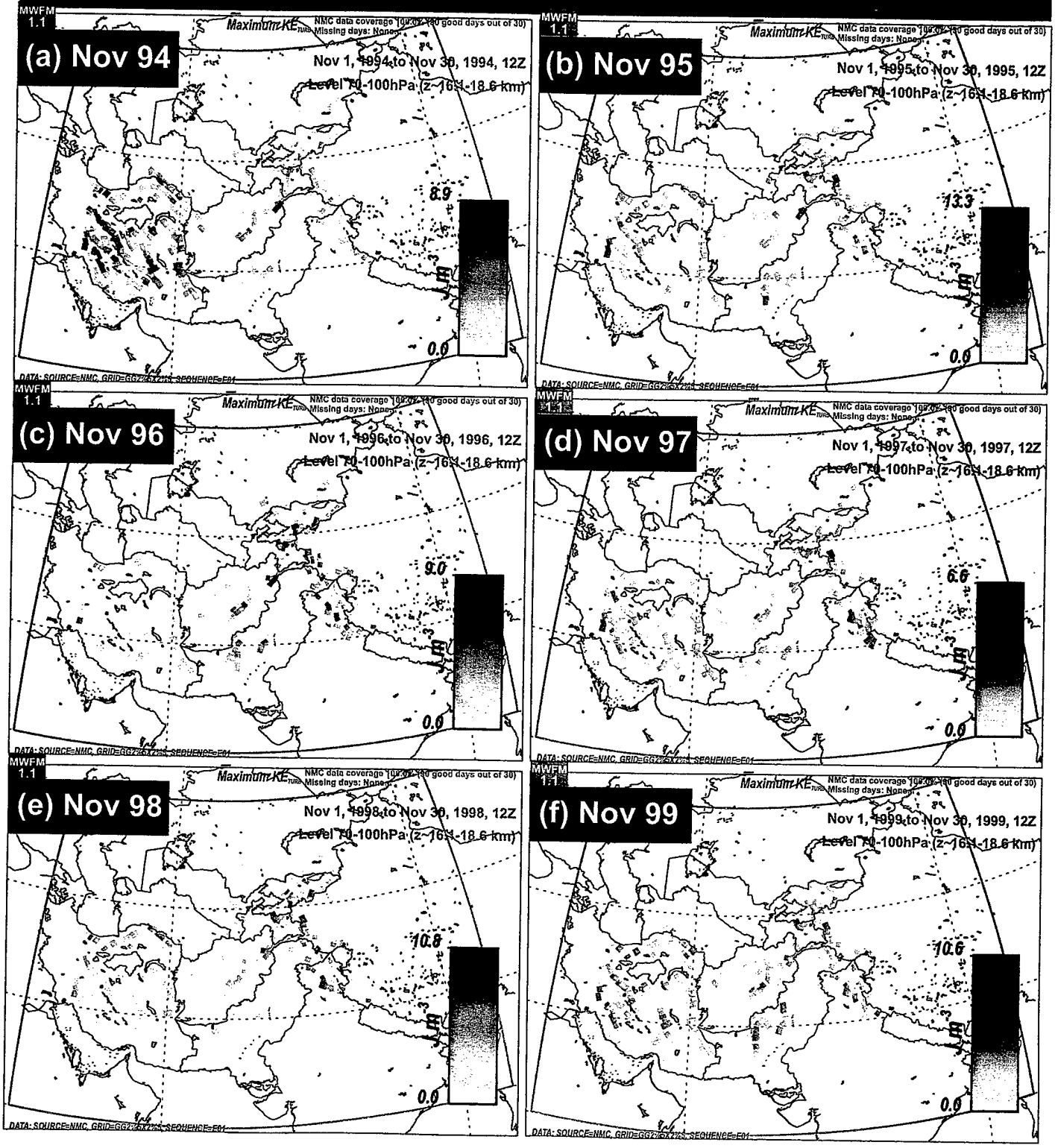

Figure 7

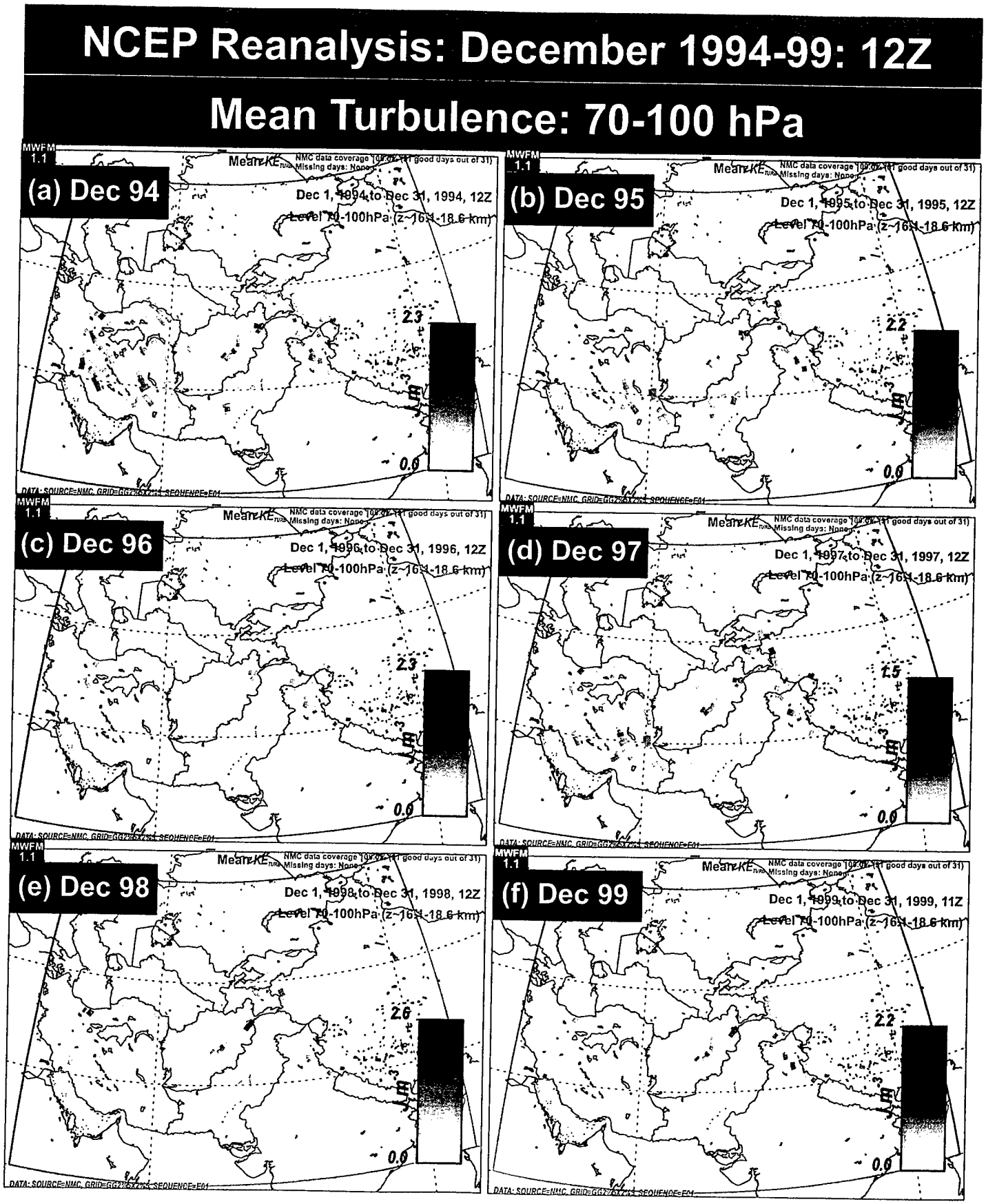
NCEP Reanalysis: December 1994-99: 12Z
Mean Turbulence: 70-100 hPa
(a) Dec 94
Dec 1, 1994 to Dec 31, 1994, 12Z
(b) Dec 95
Dec 1, 1995 to Dec 31, 1995, 12Z
(c) Dec 96
Dec 1, 1996 to Dec 31, 1996, 12Z
(d) Dec 97
Dec 1, 1997 to Dec 31, 1997, 12Z
(e) Dec 98
Dec 1, 1998 to Dec 31, 1998, 12Z
(f) Dec 99
Dec 1, 1999 to Dec 31, 1999, 11Z
Level 70-100hPa (z~16.1-18.6 km)
MWFM 1.1

Figure 8

NCEP Reanalysis: December 1994-99: 12Z

Maximum Turbulence: 70-100 hPa

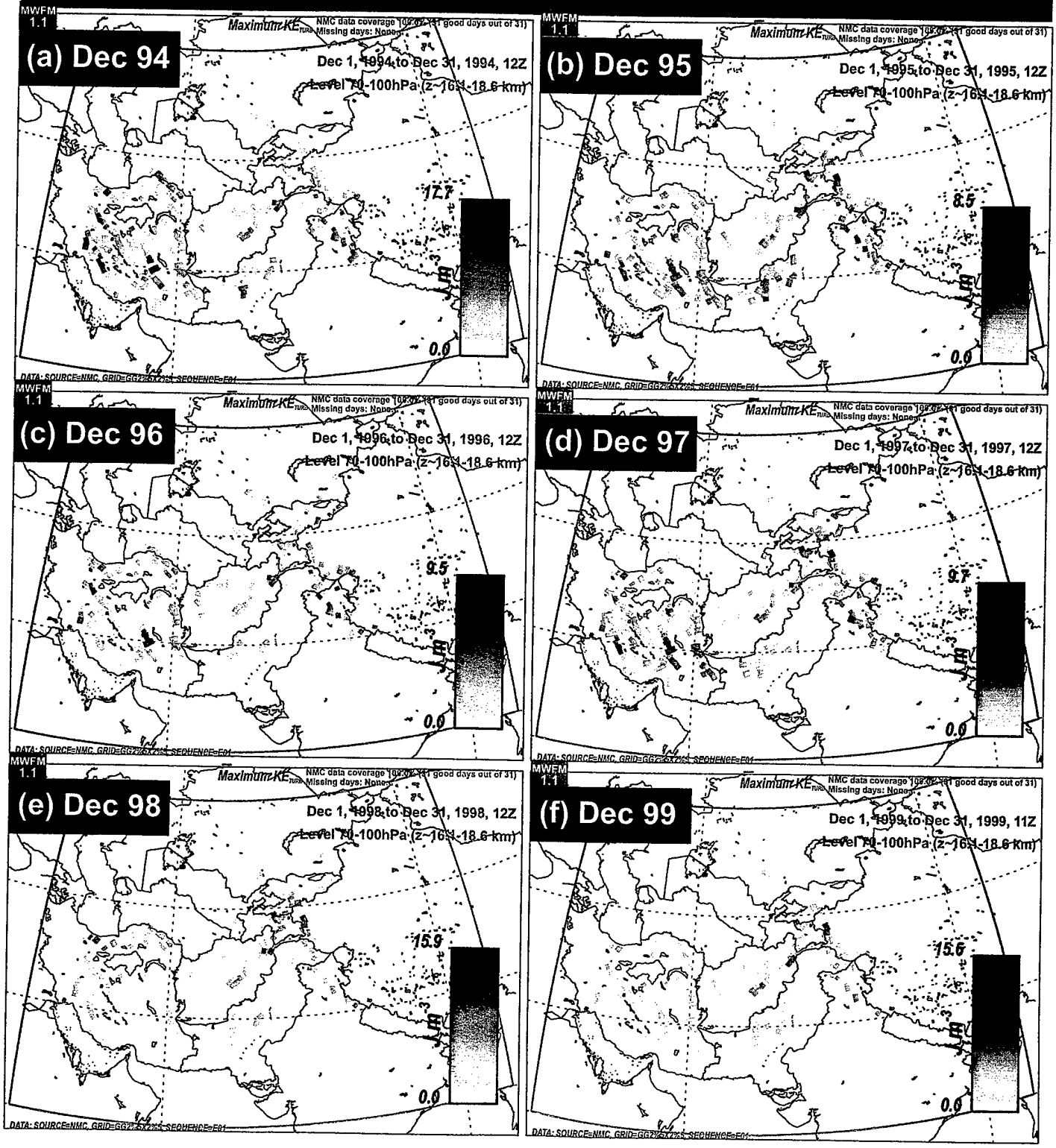

Figure 9

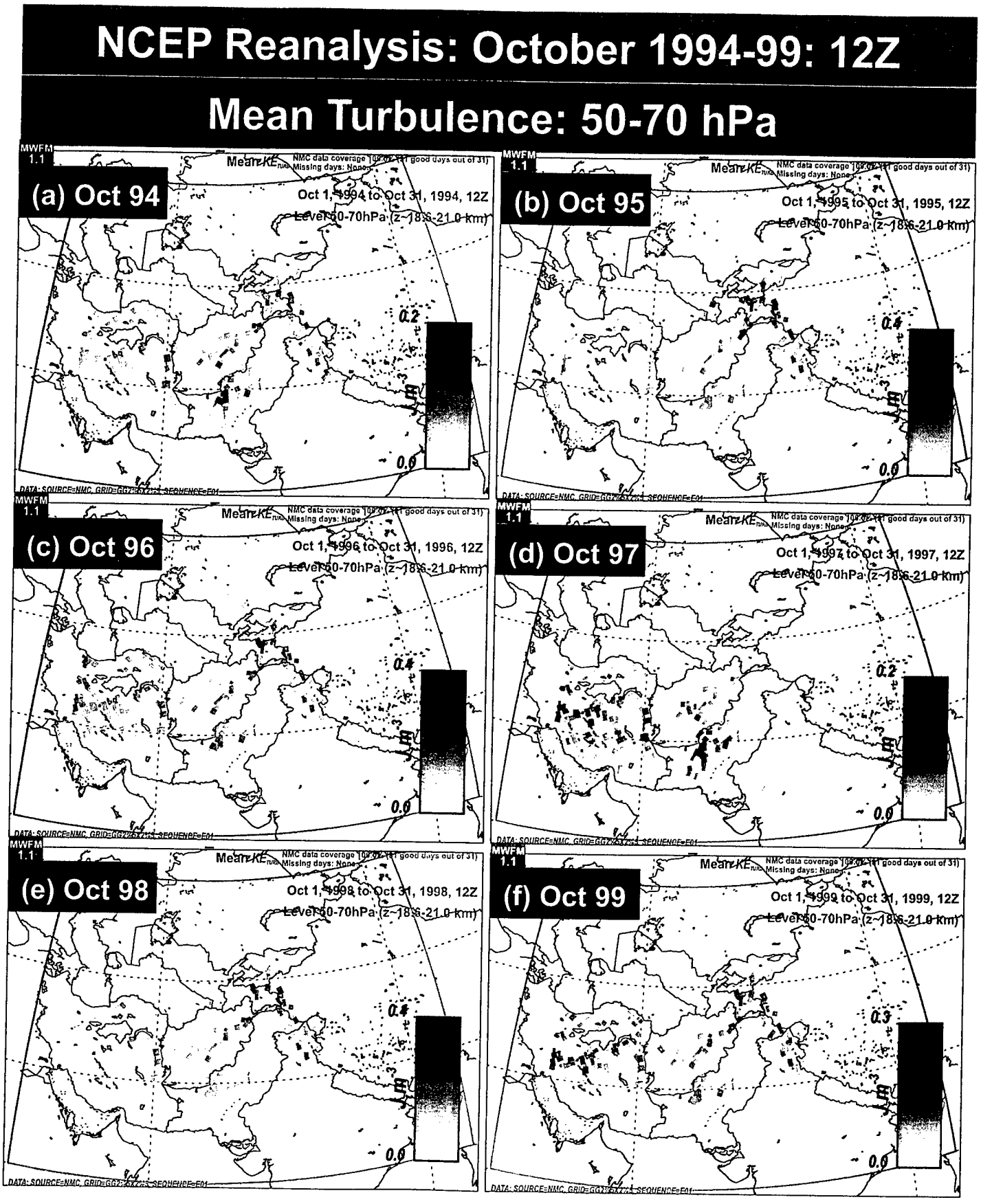
NCEP Reanalysis: October 1994-99: 12Z
Mean Turbulence: 50-70 hPa
(a) Oct 94
Oct 1, 1994 to Oct 31, 1994, 12Z
Level 50-70hPa (z~18.6-21.0 km)
(b) Oct 95
Oct 1, 1995 to Oct 31, 1995, 12Z
Level 50-70hPa (z~18.6-21.0 km)
(c) Oct 96
Oct 1, 1996 to Oct 31, 1996, 12Z
Level 50-70hPa (z~18.6-21.0 km)
(d) Oct 97
Oct 1, 1997 to Oct 31, 1997, 12Z
Level 50-70hPa (z~18.6-21.0 km)
(e) Oct 98
Oct 1, 1998 to Oct 31, 1998, 12Z
Level 50-70hPa (z~18.6-21.0 km)
(f) Oct 99
Oct 1, 1999 to Oct 31, 1999, 12Z
Level 50-70hPa (z~18.6-21.0 km)

Figure 10

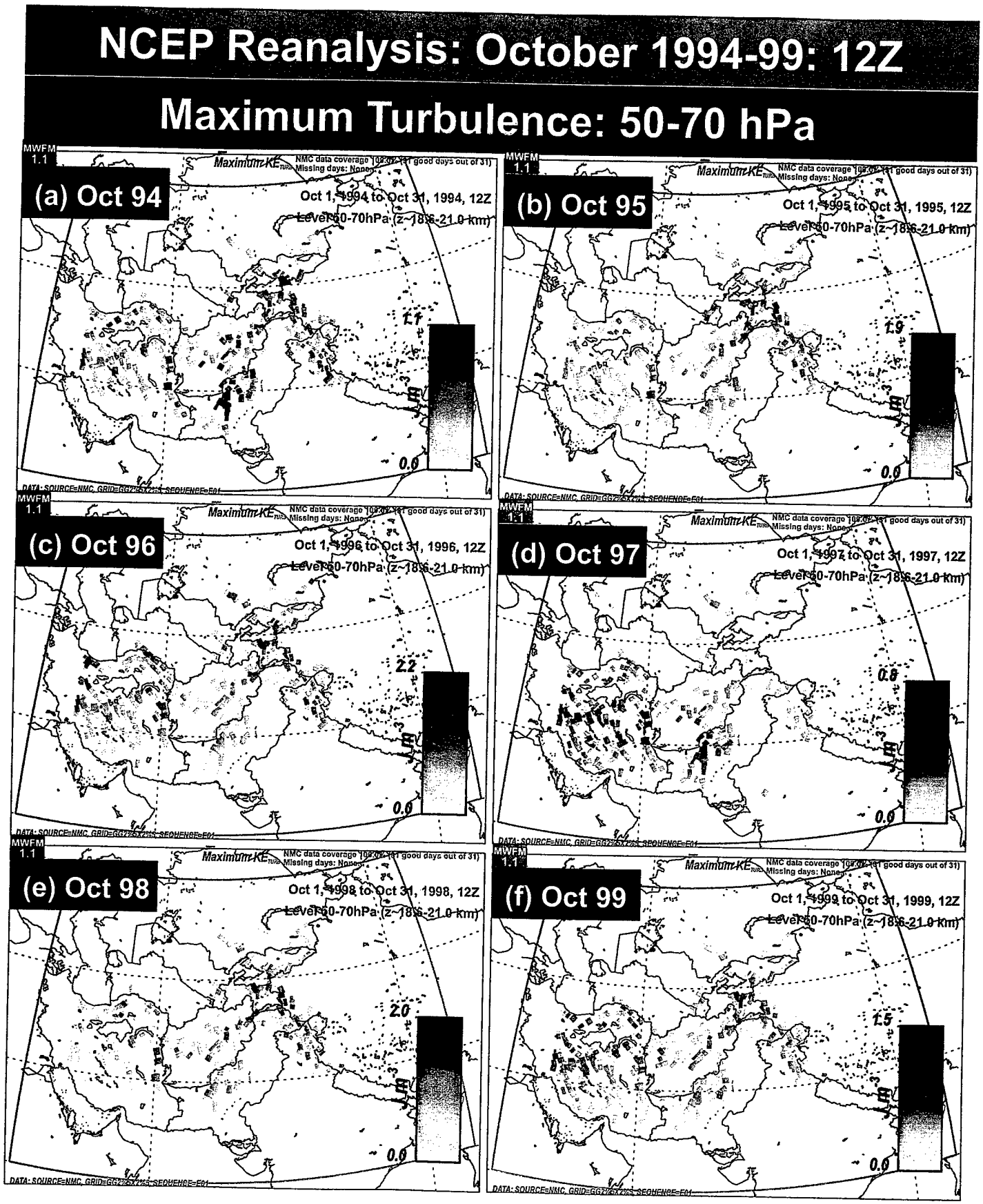
NCEP Reanalysis: October 1994-99: 12Z
Maximum Turbulence: 50-70 hPa
(a) Oct 94
Oct 1, 1994 to Oct 31, 1994, 12Z
Level 50-70hPa (z~18.6-21.0 km)
(b) Oct 95
Oct 1, 1995 to Oct 31, 1995, 12Z
Level 50-70hPa (z~18.6-21.0 km)
(c) Oct 96
Oct 1, 1996 to Oct 31, 1996, 12Z
Level 50-70hPa (z~18.6-21.0 km)
(d) Oct 97
Oct 1, 1997 to Oct 31, 1997, 12Z
Level 50-70hPa (z~18.6-21.0 km)
(e) Oct 98
Oct 1, 1998 to Oct 31, 1998, 12Z
Level 50-70hPa (z~18.6-21.0 km)
(f) Oct 99
Oct 1, 1999 to Oct 31, 1999, 12Z
Level 50-70hPa (z~18.6-21.0 km)

Figure 11

NCEP Reanalysis: November 1994-99: 12Z

Mean Turbulence: 50-70 hPa

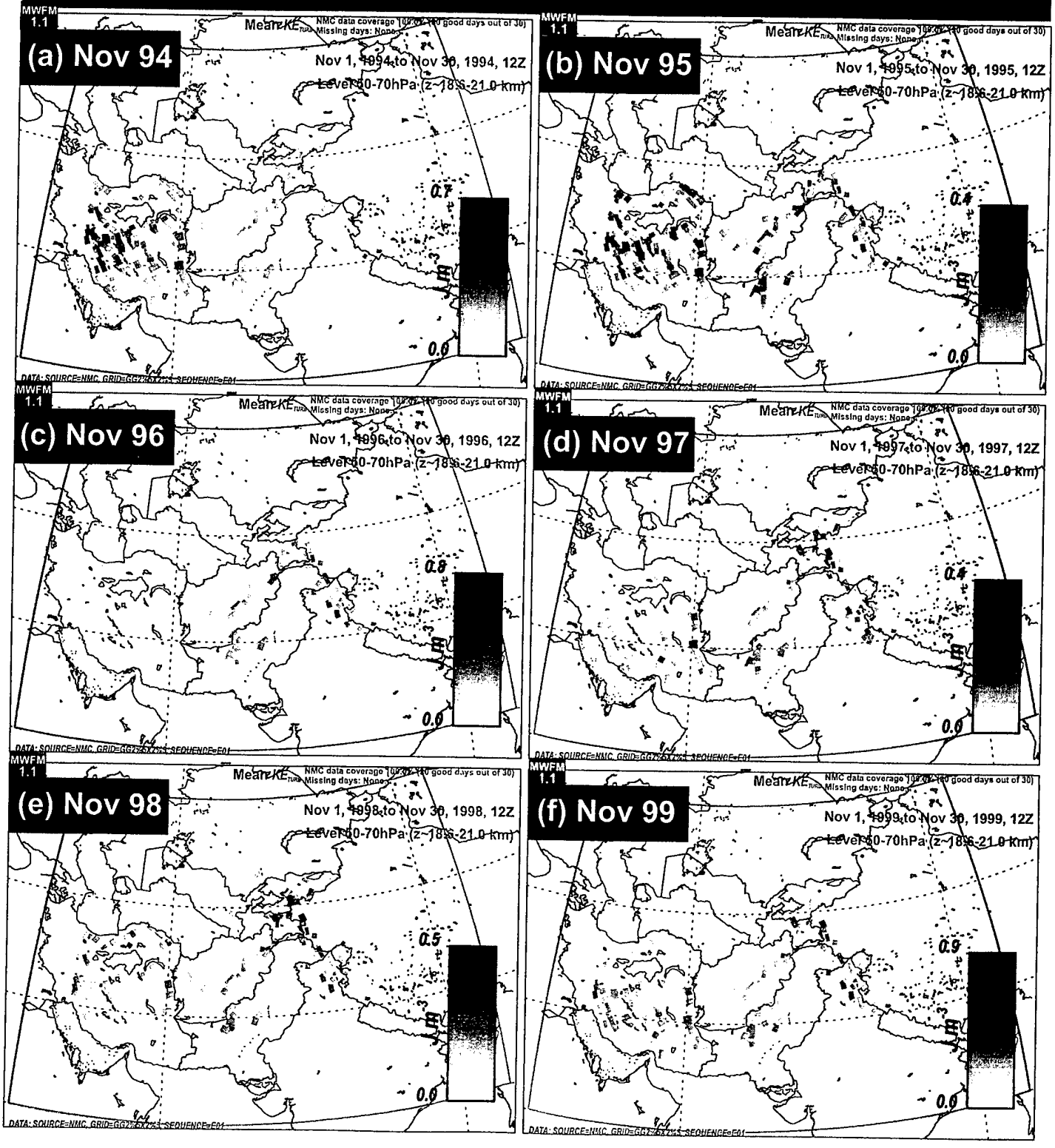

Figure 12

NCEP Reanalysis: November 1994-99: 12Z

Maximum Turbulence: 50-70 hPa

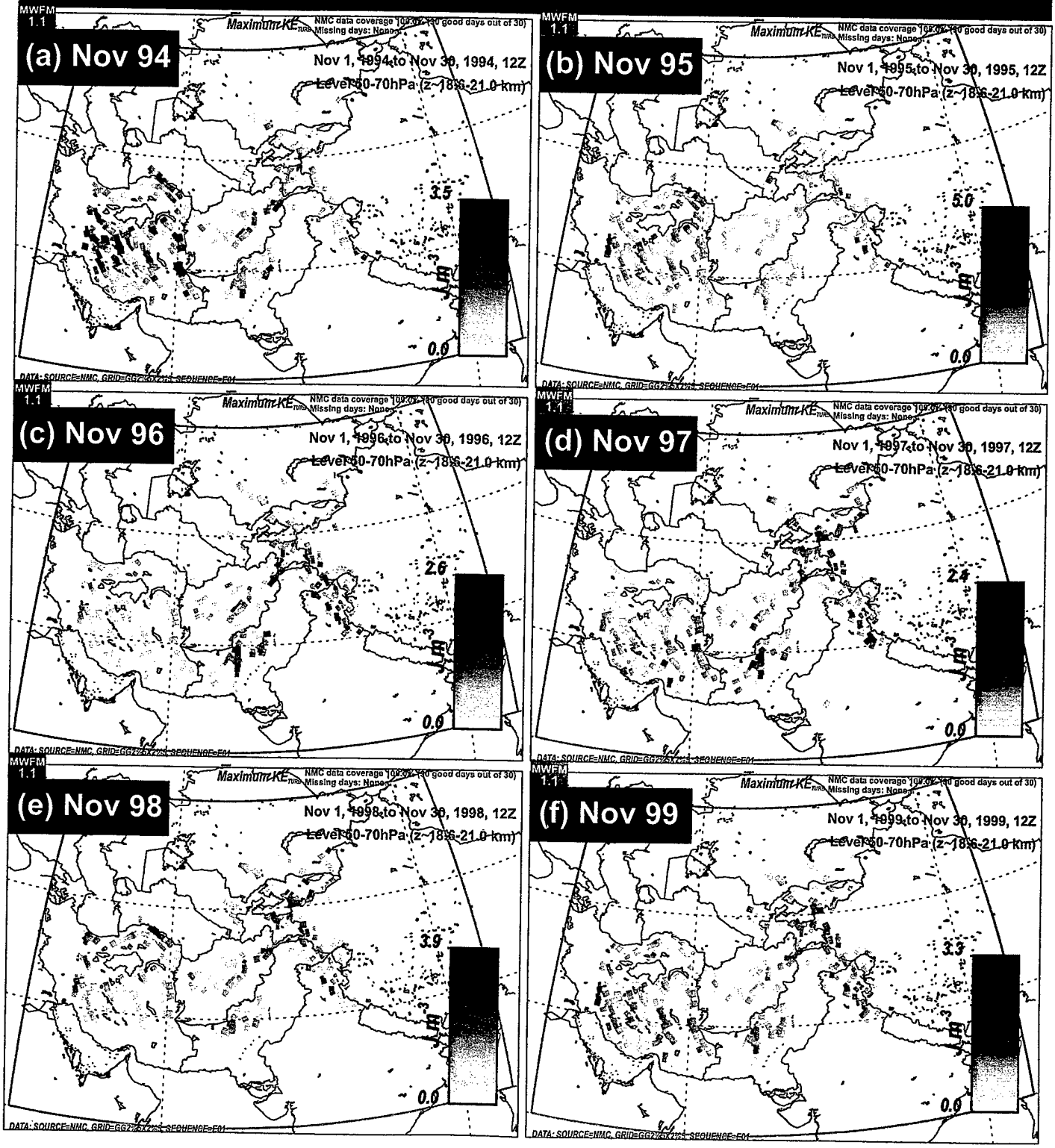

Figure 13

NCEP Reanalysis: December 1994-99: 12Z

Mean Turbulence: 50-70 hPa

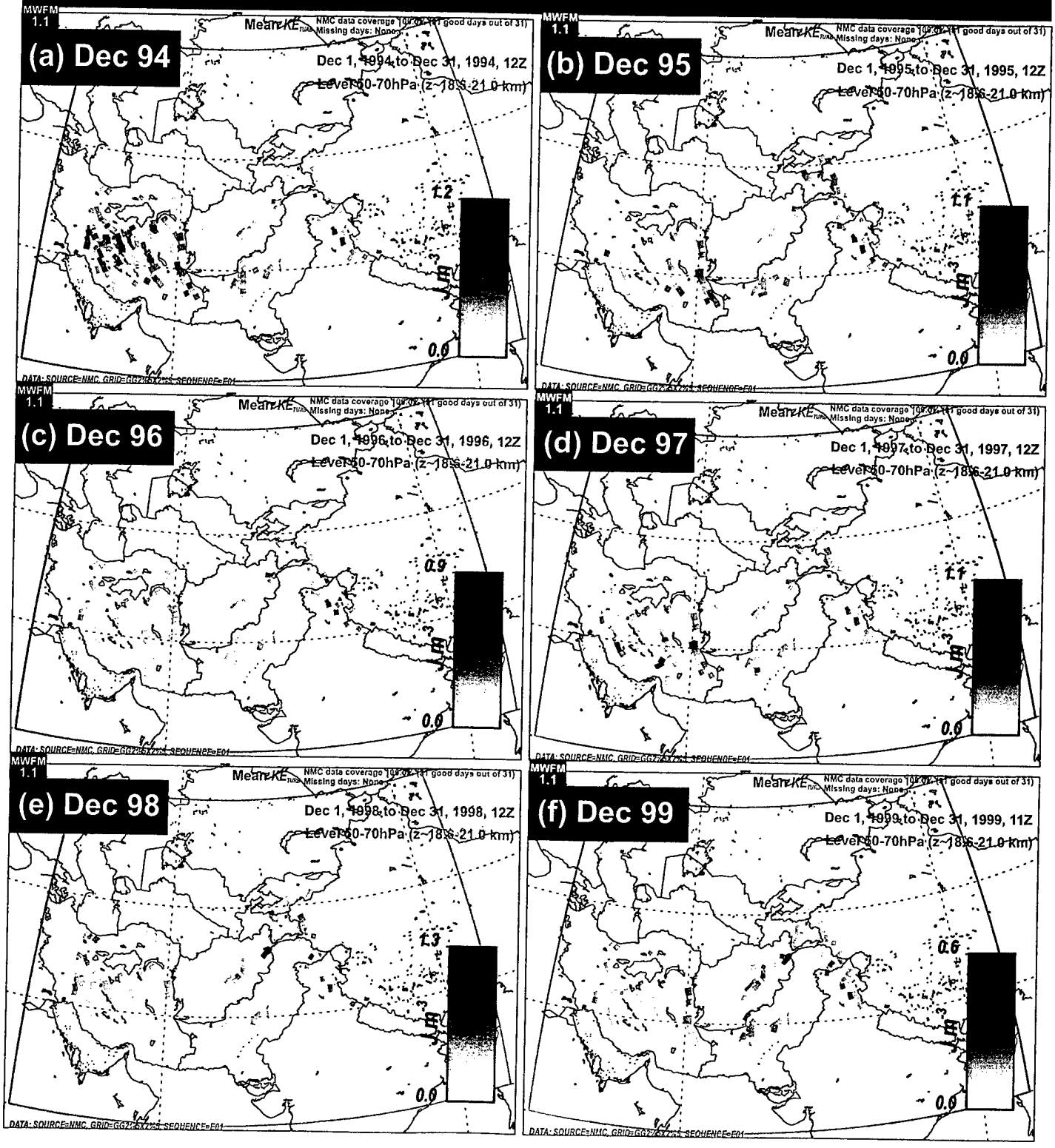

Figure 14

NCEP Reanalysis: December 1994-99: 12Z

Maximum Turbulence: 50-70 hPa

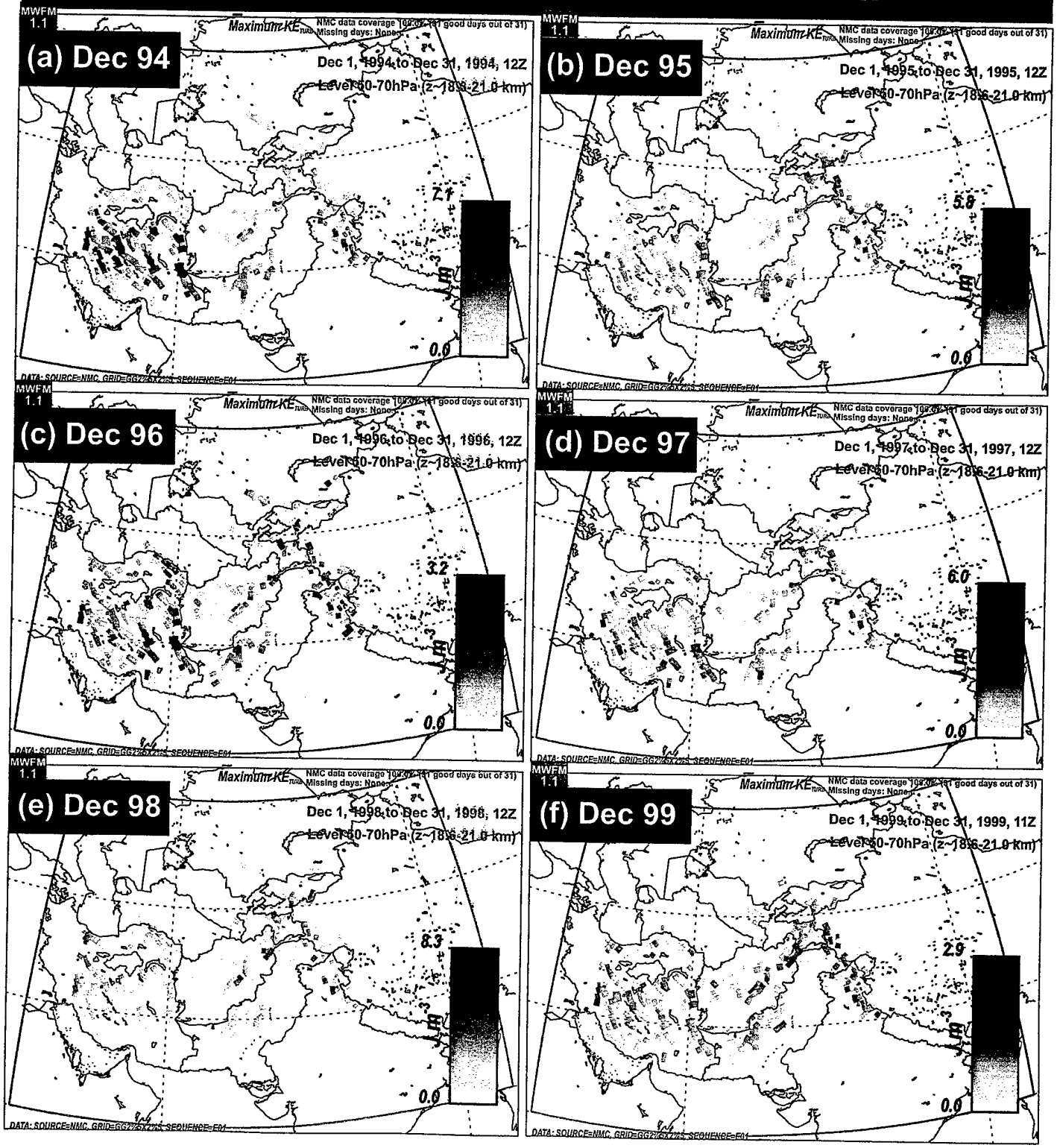

Figure 15

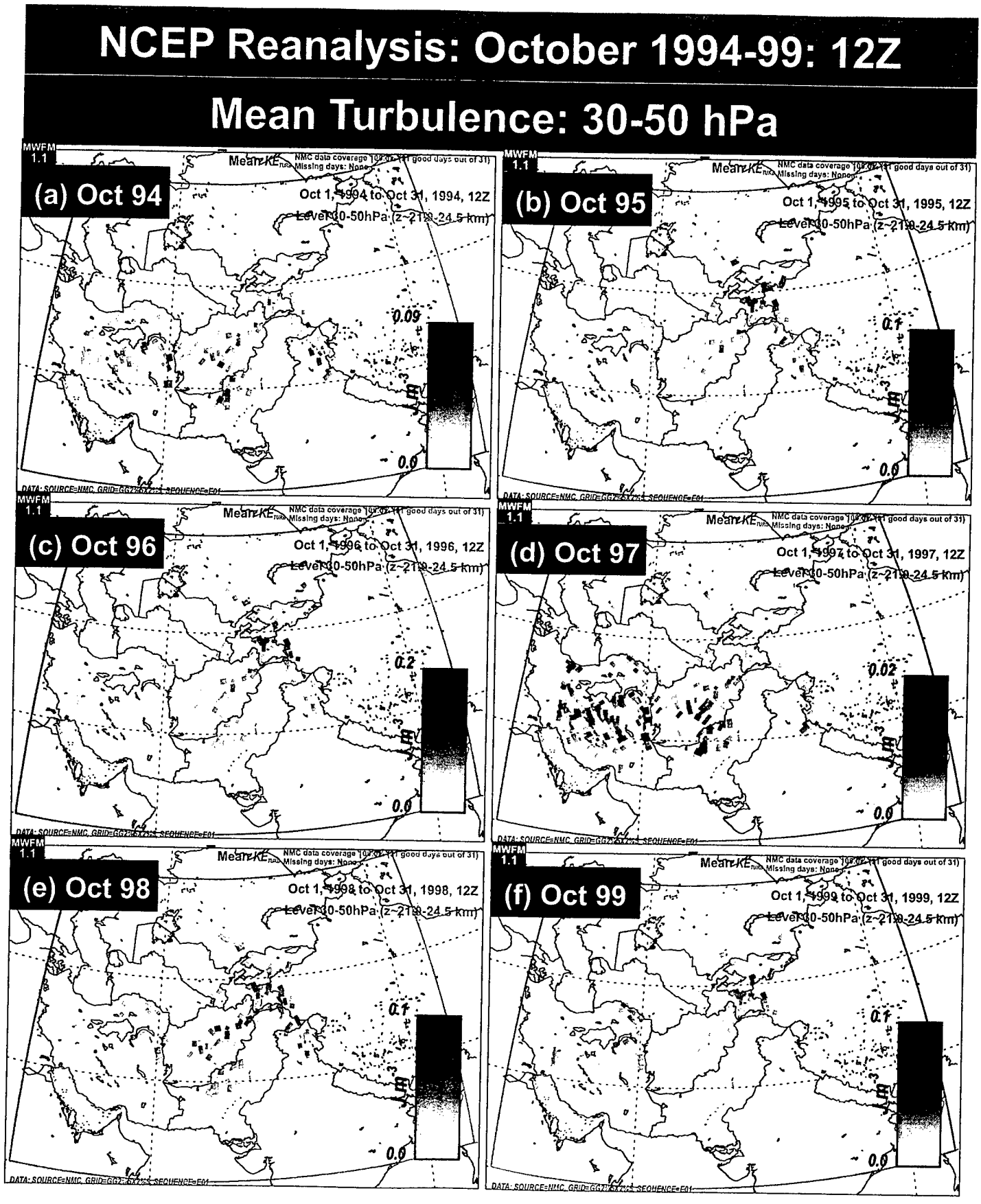
NCEP Reanalysis: October 1994-99: 12Z
Mean Turbulence: 30-50 hPa
(a) Oct 94
Oct 1, 1994 to Oct 31, 1994, 12Z
Level 30-50hPa (z~21.9-24.5 km)
0.09
0.0
(b) Oct 95
Oct 1, 1995 to Oct 31, 1995, 12Z
Level 30-50hPa (z~21.9-24.5 km)
0.1
0.0
(c) Oct 96
Oct 1, 1996 to Oct 31, 1996, 12Z
Level 30-50hPa (z~21.9-24.5 km)
0.2
0.0
(d) Oct 97
Oct 1, 1997 to Oct 31, 1997, 12Z
Level 30-50hPa (z~21.9-24.5 km)
0.02
0.0
(e) Oct 98
Oct 1, 1998 to Oct 31, 1998, 12Z
Level 30-50hPa (z~21.9-24.5 km)
0.1
0.0
(f) Oct 99
Oct 1, 1999 to Oct 31, 1999, 12Z
Level 30-50hPa (z~21.9-24.5 km)
0.1
0.0

Figure 16

NCEP Reanalysis: October 1994-99: 12Z

Maximum Turbulence: 30-50 hPa

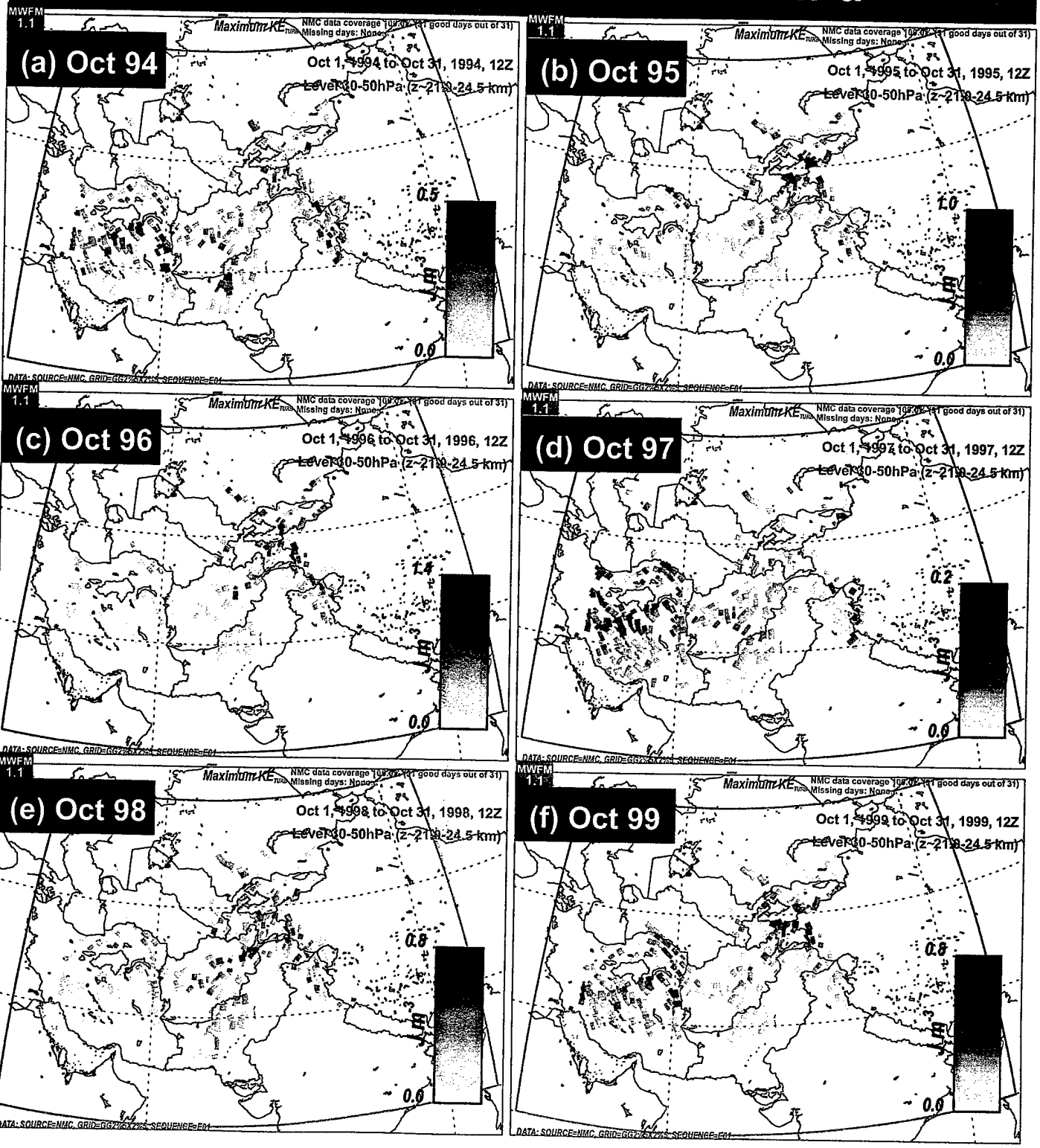

Figure 17

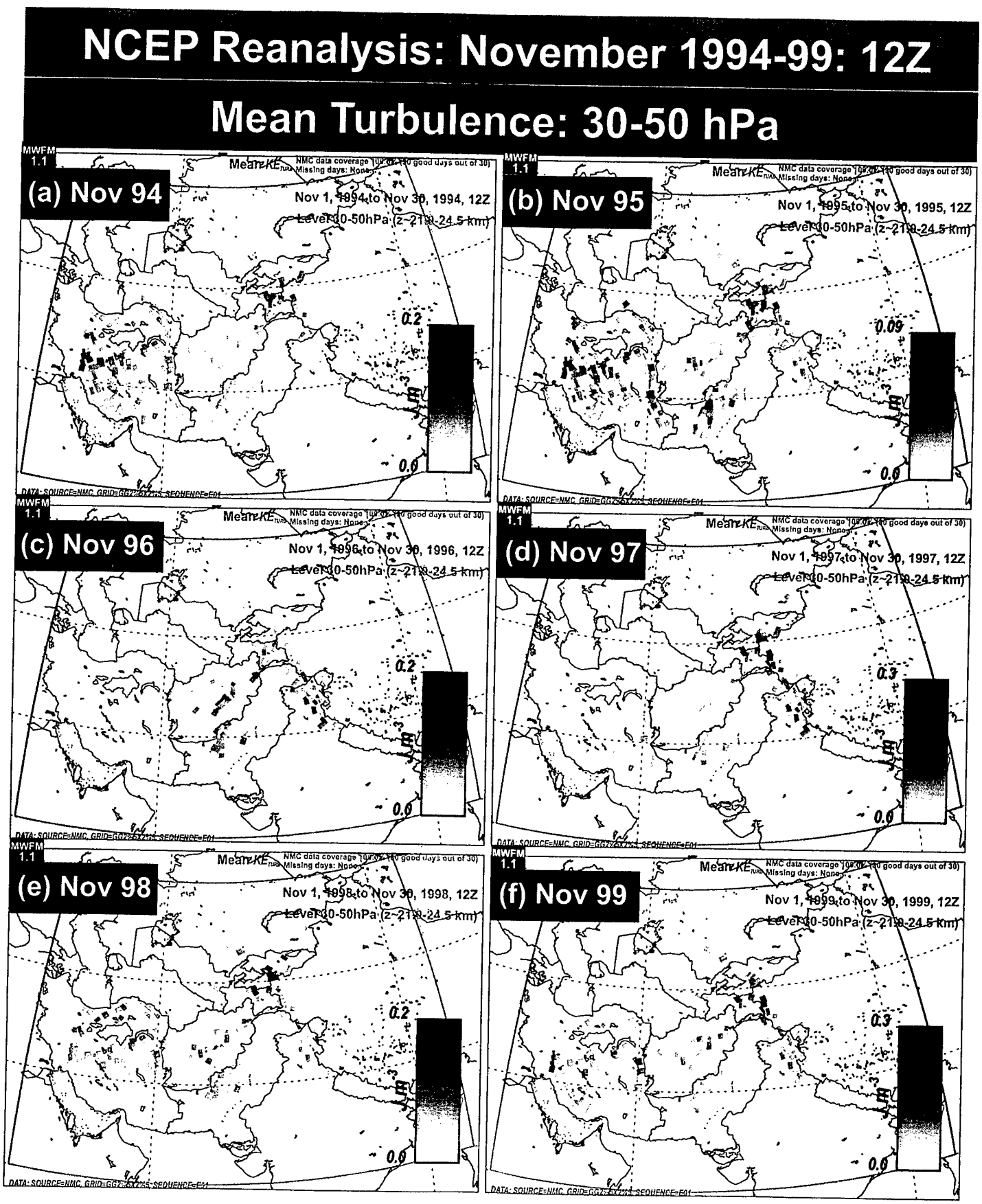
NCEP Reanalysis: November 1994-99: 12Z
Mean Turbulence: 30-50 hPa
(a) Nov 94
Nov 1, 1994 to Nov 30, 1994, 12Z
(b) Nov 95
Nov 1, 1995 to Nov 30, 1995, 12Z
(c) Nov 96
Nov 1, 1996 to Nov 30, 1996, 12Z
(d) Nov 97
Nov 1, 1997 to Nov 30, 1997, 12Z
(e) Nov 98
Nov 1, 1998 to Nov 30, 1998, 12Z
(f) Nov 99
Nov 1, 1999 to Nov 30, 1999, 12Z
Level 30-50hPa (z~21.9-24.5 km)
MWFM 1.1
NMC data coverage 100.0% (30 good days out of 30)
Missing days: None
0.2
0.09
0.3
0.0

Figure 18

NCEP Reanalysis: November 1994-99: 12Z

Maximum Turbulence: 30-50 hPa

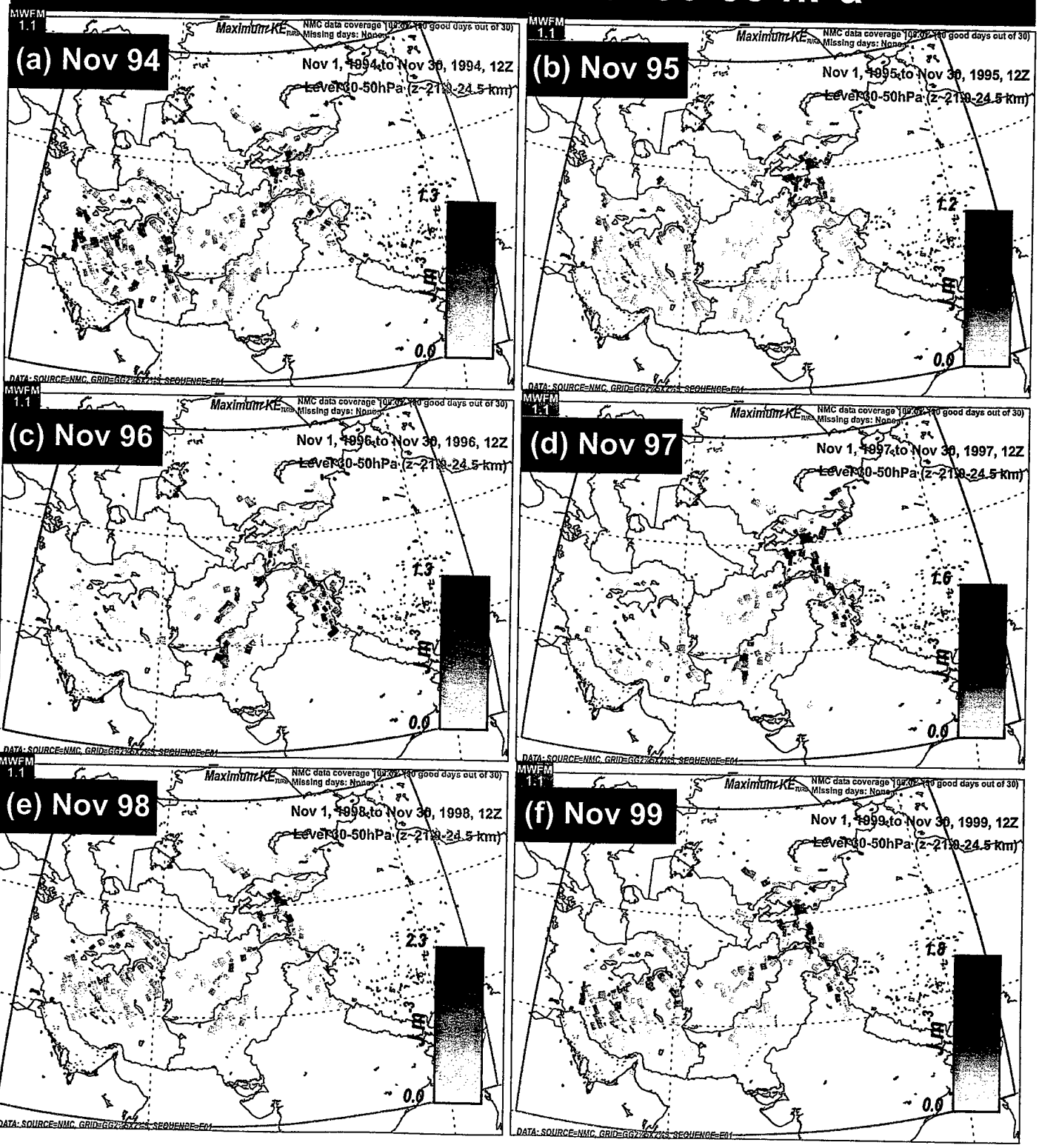

Figure 19

NCEP Reanalysis: December 1994-99: 12Z

Mean Turbulence: 30-50 hPa

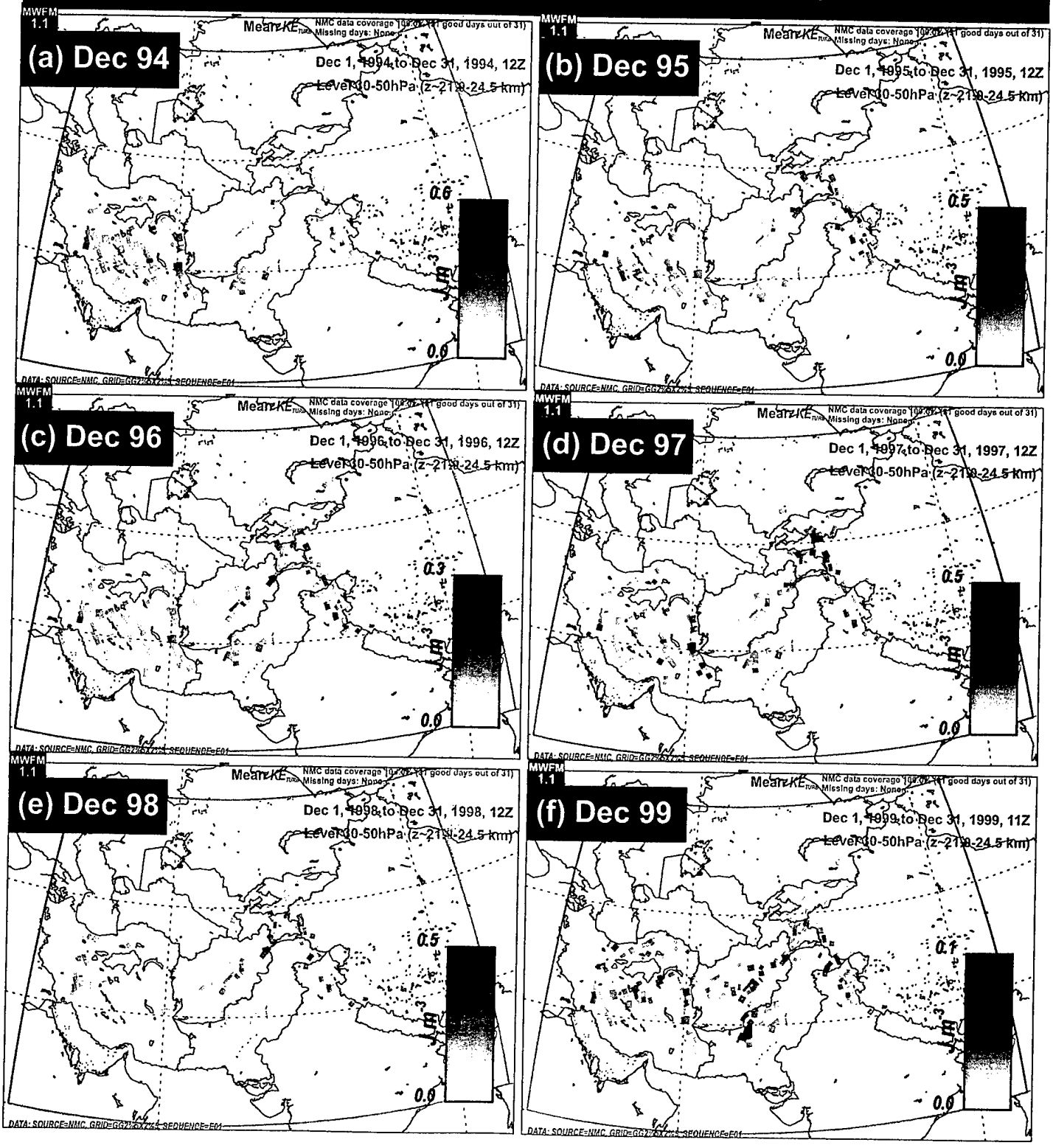

Figure 20

NCEP Reanalysis: December 1994-99: 12Z

Maximum Turbulence: 30-50 hPa

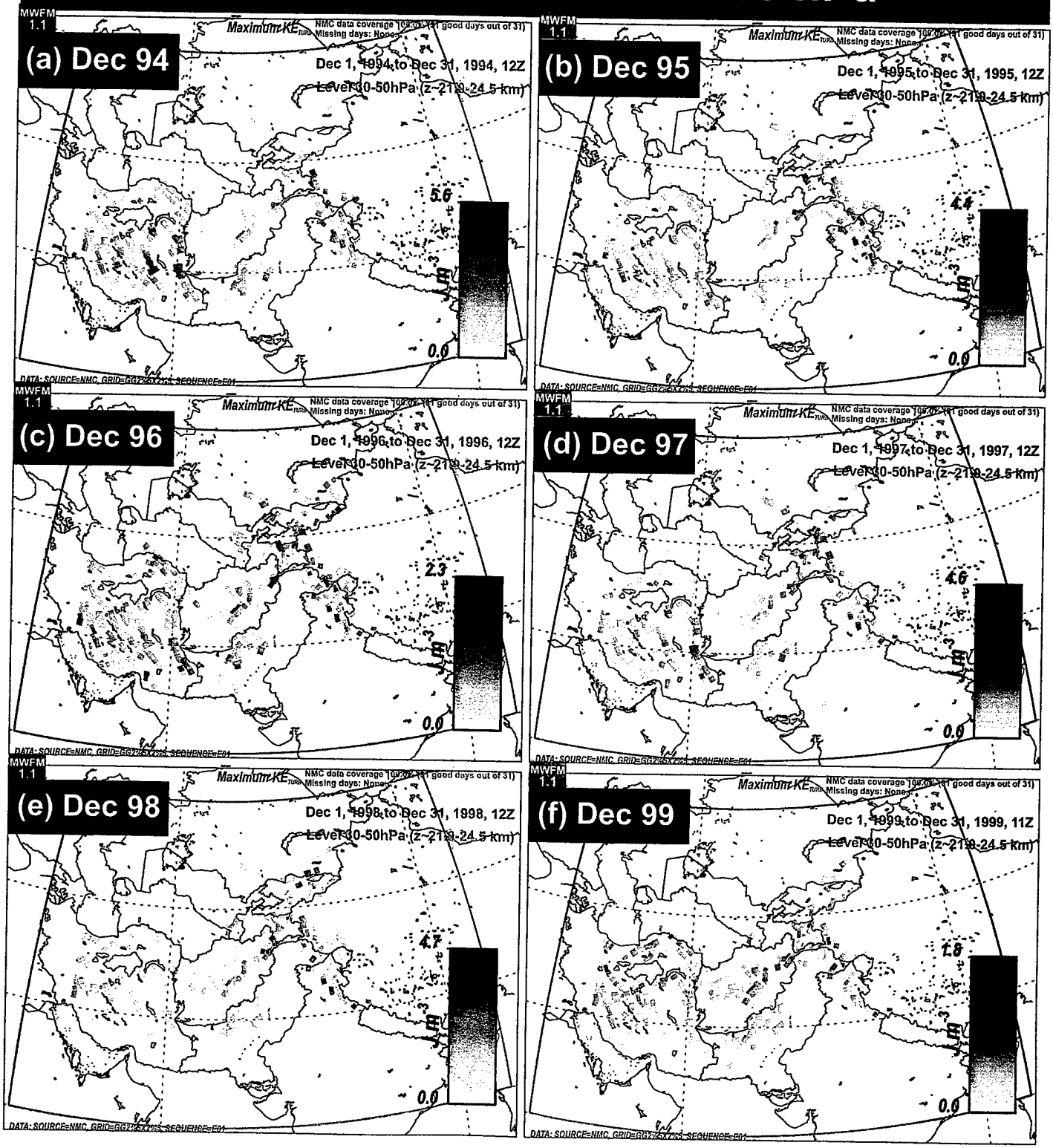

Figure 21

DAO Analysis: October 1994-97: 12Z

Mean Turbulence: 70-100 hPa

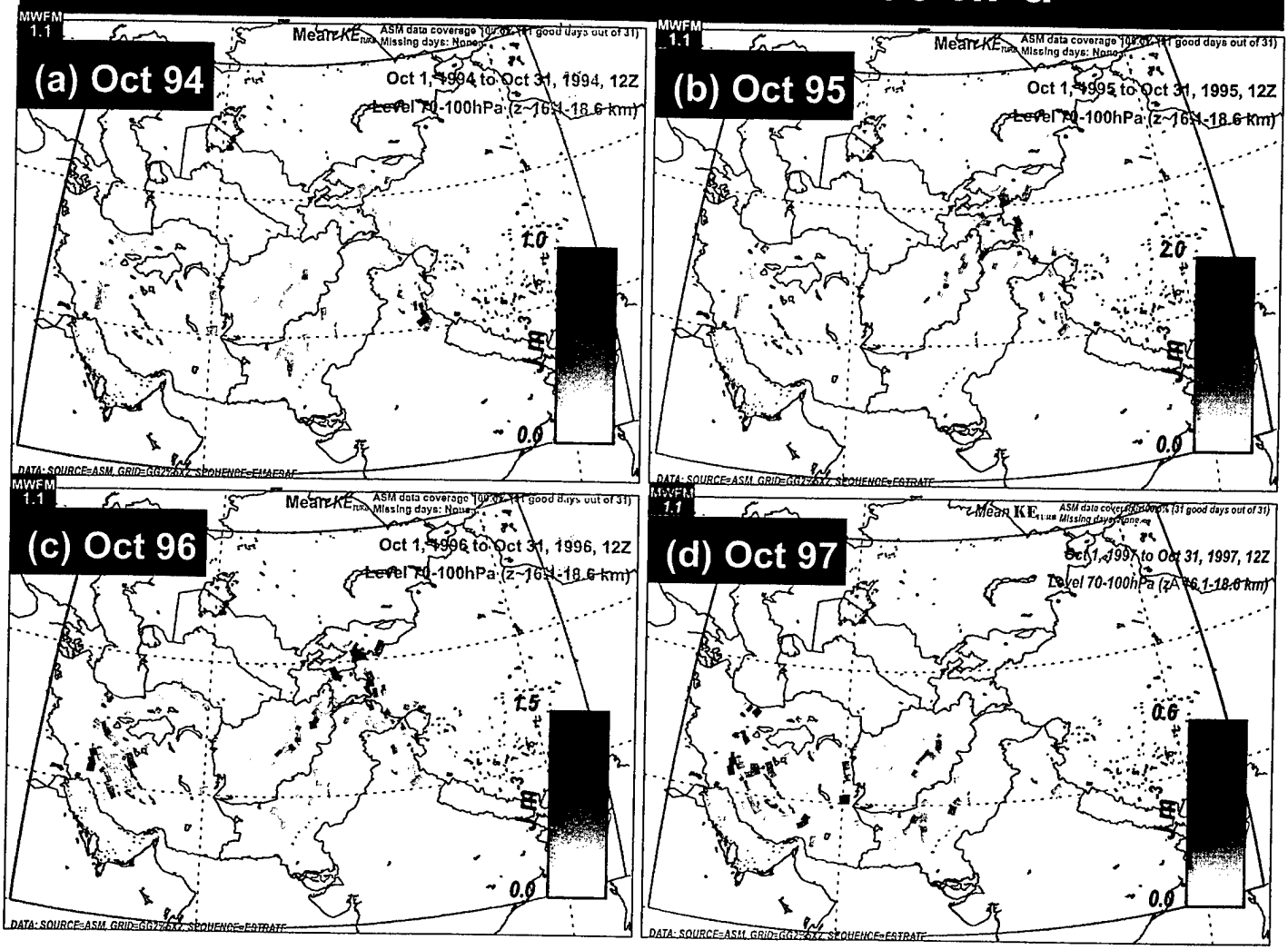

Figure 22

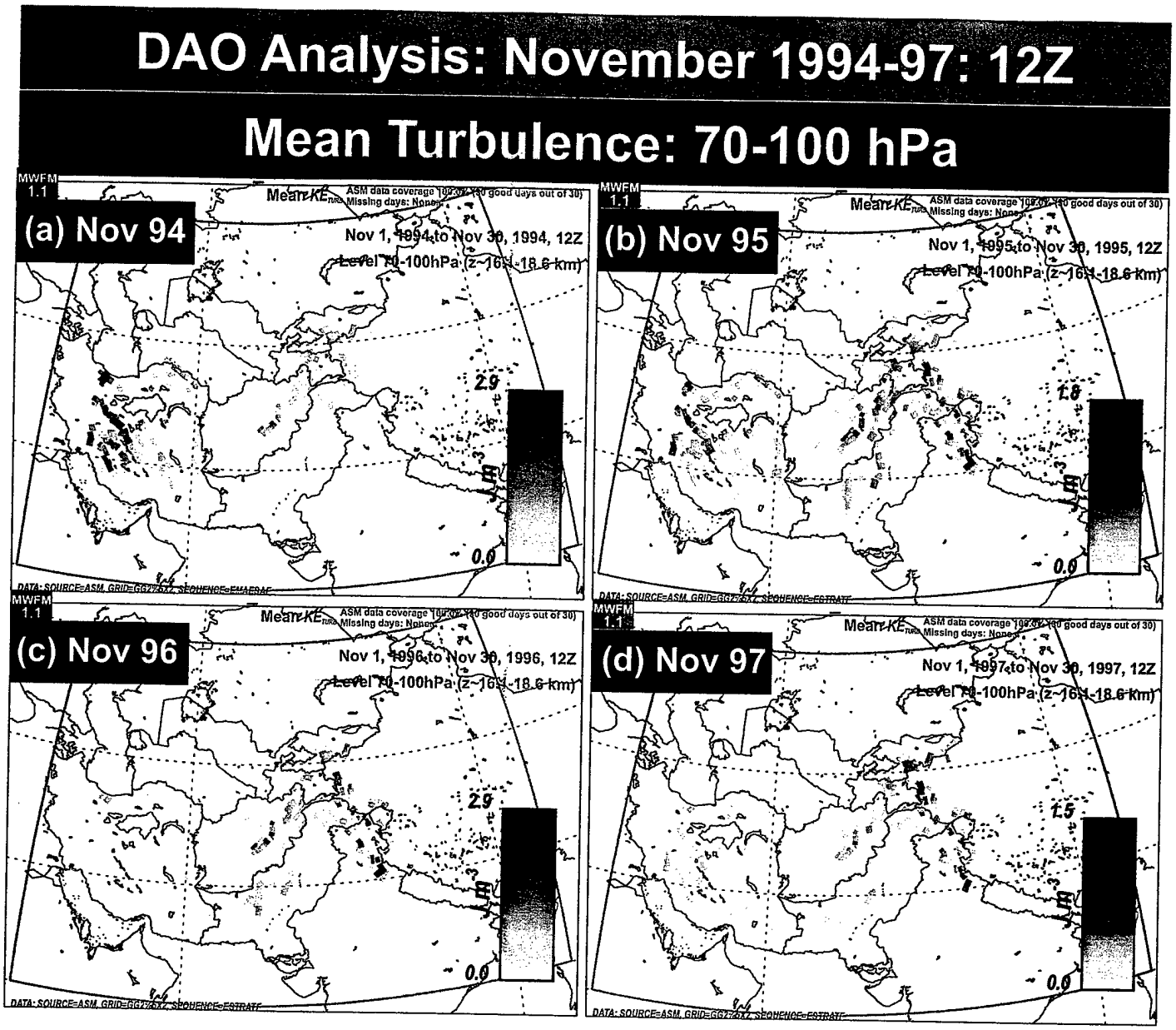
DAO Analysis: November 1994-97: 12Z
Mean Turbulence: 70-100 hPa
(a) Nov 94
Nov 1, 1994 to Nov 30, 1994, 12Z
Level 70-100hPa (z~16.1-18.6 km)
(b) Nov 95
Nov 1, 1995 to Nov 30, 1995, 12Z
Level 70-100hPa (z~16.1-18.6 km)
(c) Nov 96
Nov 1, 1996 to Nov 30, 1996, 12Z
Level 70-100hPa (z~16.1-18.6 km)
(d) Nov 97
Nov 1, 1997 to Nov 30, 1997, 12Z
Level 70-100hPa (z~16.1-18.6 km)

Figure 23

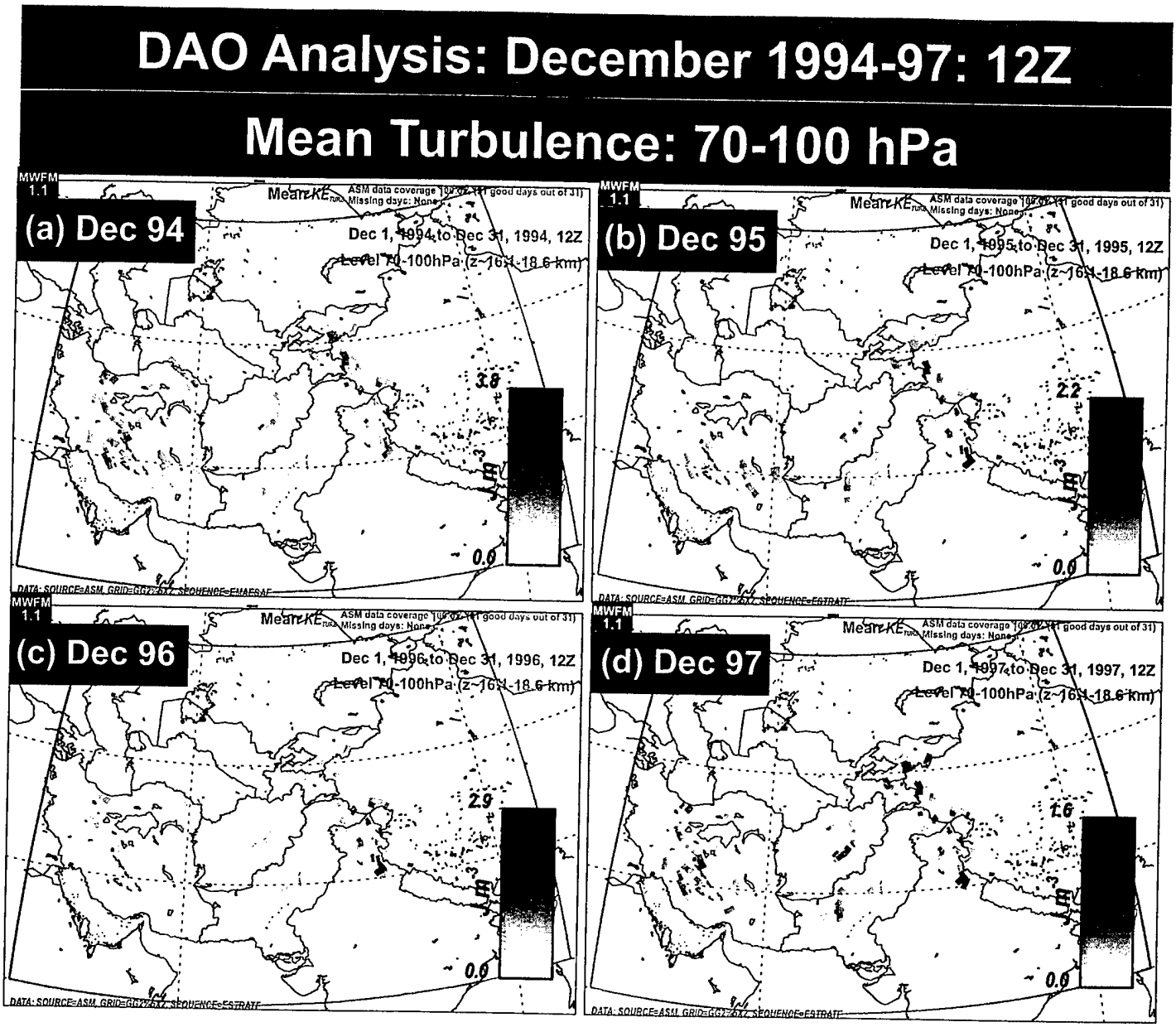
DAO Analysis: December 1994-97: 12Z
Mean Turbulence: 70-100 hPa
(a) Dec 94
Dec 1, 1994 to Dec 31, 1994, 12Z
Level 70-100hPa (z~16.1-18.6 km)
3.8
0.0
(b) Dec 95
Dec 1, 1995 to Dec 31, 1995, 12Z
Level 70-100hPa (z~16.1-18.6 km)
2.2
0.0
(c) Dec 96
Dec 1, 1996 to Dec 31, 1996, 12Z
Level 70-100hPa (z~16.1-18.6 km)
2.9
0.0
(d) Dec 97
Dec 1, 1997 to Dec 31, 1997, 12Z
Level 70-100hPa (z~16.1-18.6 km)
1.6
0.0

Figure 24

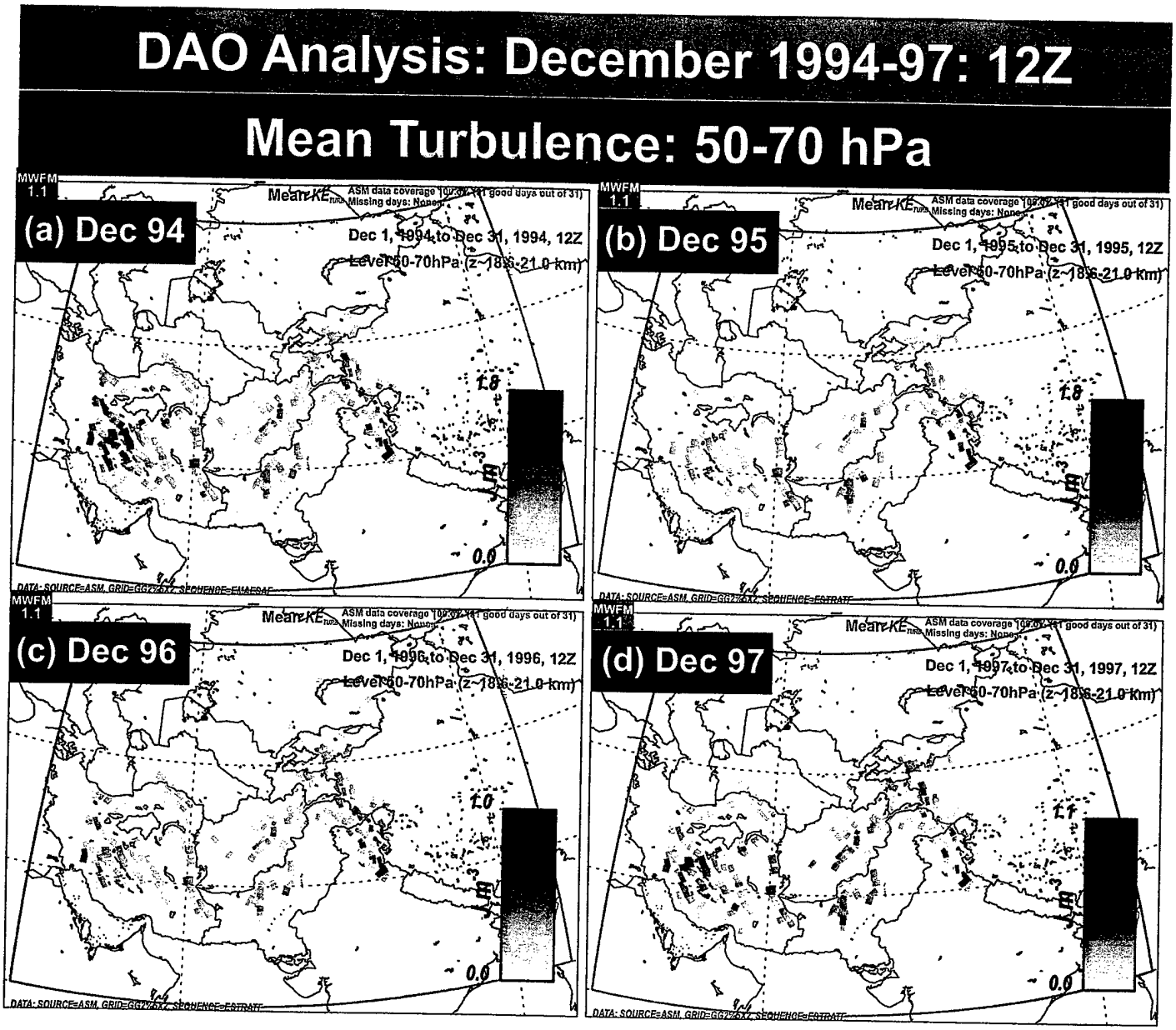
DAO Analysis: December 1994-97: 12Z
Mean Turbulence: 50-70 hPa
MWFM 1.1
(a) Dec 94
Mean KE_{turb}
ASM data coverage 100.0% (31 good days out of 31)
Missing days: None
Dec 1, 1994 to Dec 31, 1994, 12Z
Level 50-70hPa (z ~18.6-21.0 km)
1.8
0.0
DATA: SOURCE=ASM, GRID=GG2°x2°, SEQUENCE=FMAFOAF
MWFM 1.1
(b) Dec 95
Mean KE_{turb}
ASM data coverage 100.0% (31 good days out of 31)
Missing days: None
Dec 1, 1995 to Dec 31, 1995, 12Z
Level 50-70hPa (z ~18.6-21.0 km)
1.8
0.0
DATA: SOURCE=ASM, GRID=GG2°x2°, SEQUENCE=FOTRATF
MWFM 1.1
(c) Dec 96
Mean KE_{turb}
ASM data coverage 100.0% (31 good days out of 31)
Missing days: None
Dec 1, 1996 to Dec 31, 1996, 12Z
Level 50-70hPa (z ~18.6-21.0 km)
1.0
0.0
DATA: SOURCE=ASM, GRID=GG2°x2°, SEQUENCE=FOTRATF
MWFM 1.1
(d) Dec 97
Mean KE_{turb}
ASM data coverage 100.0% (31 good days out of 31)
Missing days: None
Dec 1, 1997 to Dec 31, 1997, 12Z
Level 50-70hPa (z ~18.6-21.0 km)
1.1
0.0
DATA: SOURCE=ASM, GRID=GG2°x2°, SEQUENCE=FOTRATF

Figure 25

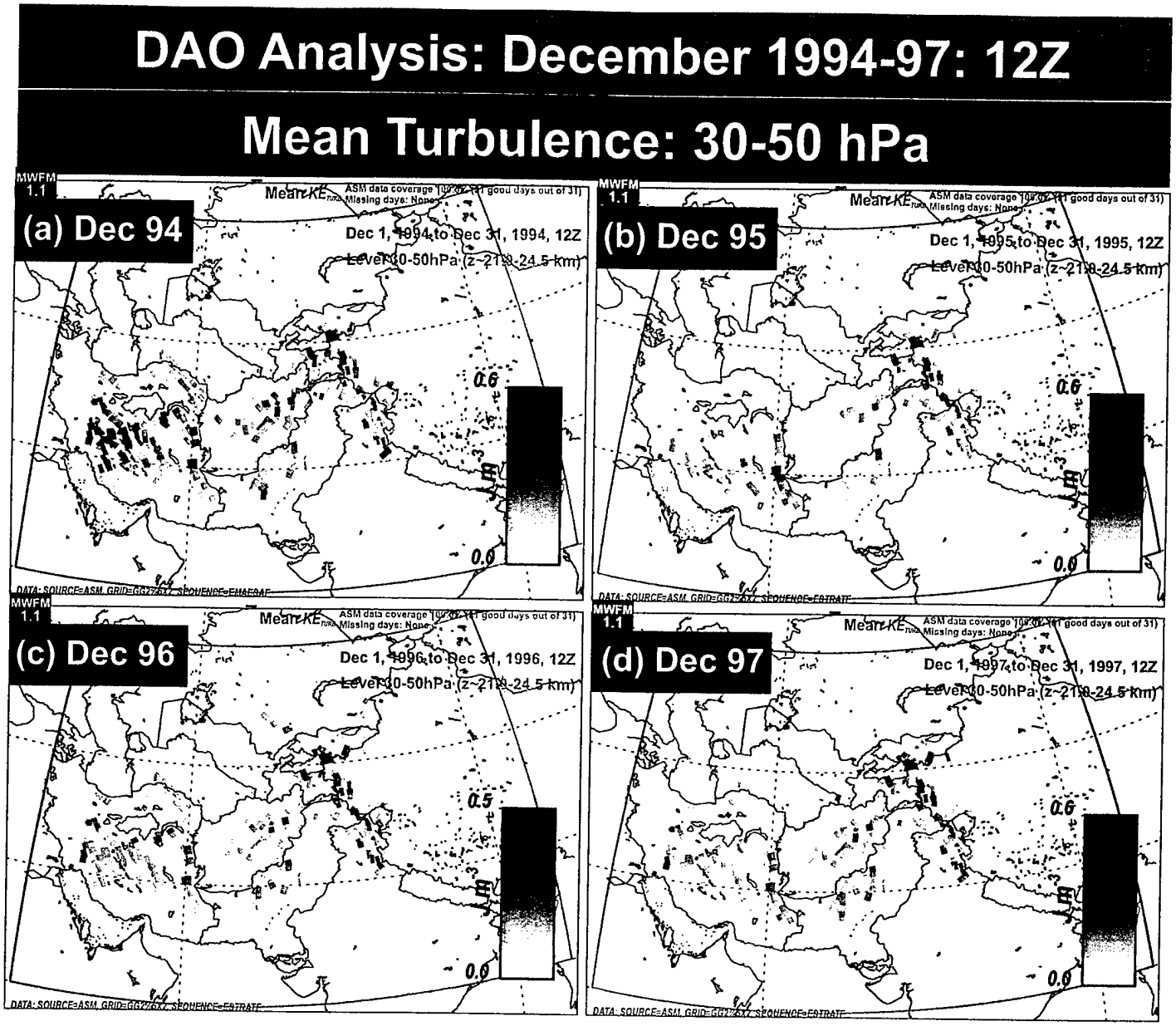
DAO Analysis: December 1994-97: 12Z
Mean Turbulence: 30-50 hPa
MWFM 1.1
(a) Dec 94
Mean EKE_{TURB}
ASM data coverage [100.0%, 31 good days out of 31]
Missing days: None
Dec 1, 1994 to Dec 31, 1994, 12Z
Level: 30-50hPa (z~21.9-24.5 km)
0.6
0.0
DATA: SOURCE=ASM, GRID=GG72.5X2, SEQUENCE=EMAEOAF
MWFM 1.1
(b) Dec 95
Mean EKE_{TURB}
ASM data coverage [100.0%, 31 good days out of 31]
Missing days: None
Dec 1, 1995 to Dec 31, 1995, 12Z
Level: 30-50hPa (z~21.9-24.5 km)
0.6
0.0
DATA: SOURCE=ASM, GRID=GG72.5X2, SEQUENCE=E0TRATF
MWFM 1.1
(c) Dec 96
Mean EKE_{TURB}
ASM data coverage [100.0%, 31 good days out of 31]
Missing days: None
Dec 1, 1996 to Dec 31, 1996, 12Z
Level: 30-50hPa (z~21.9-24.5 km)
0.5
0.0
DATA: SOURCE=ASM, GRID=GG72.5X2, SEQUENCE=E0TRATF
MWFM 1.1
(d) Dec 97
Mean EKE_{TURB}
ASM data coverage [100.0%, 31 good days out of 31]
Missing days: None
Dec 1, 1997 to Dec 31, 1997, 12Z
Level: 30-50hPa (z~21.9-24.5 km)
0.6
0.0
DATA: SOURCE=ASM, GRID=GG72.5X2, SEQUENCE=E0TRATF

Figure 26

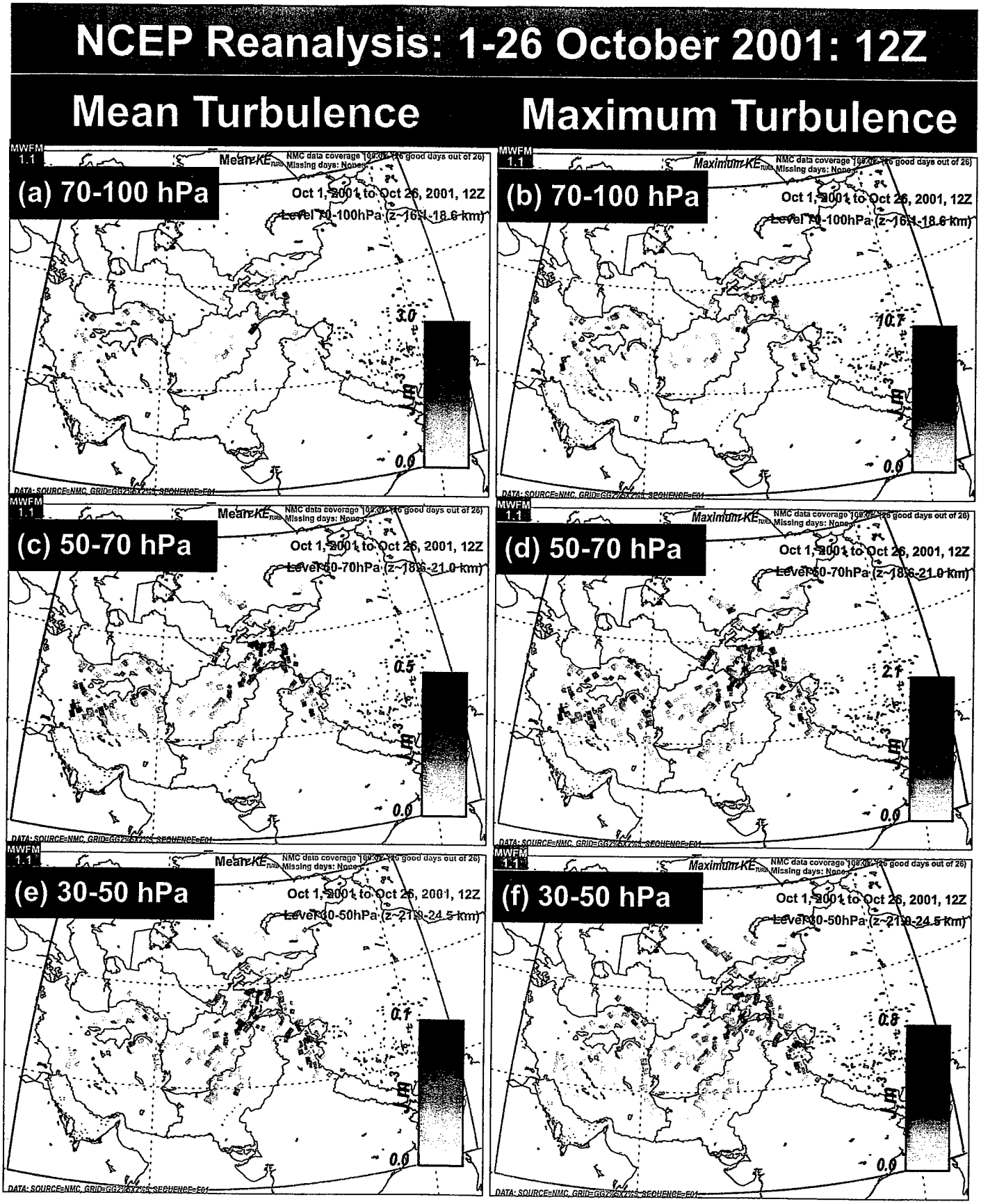
NCEP Reanalysis: 1-26 October 2001: 12Z
Mean Turbulence
Maximum Turbulence
(a) 70-100 hPa
(b) 70-100 hPa
(c) 50-70 hPa
(d) 50-70 hPa
(e) 30-50 hPa
(f) 30-50 hPa
Oct 1, 2001 to Oct 26, 2001, 12Z
Missing days: None
3.0
10.7
0.5
2.1
0.1
0.8
0.0

Figure C.1